



Lawrence Berkeley Laboratory

UNIVERSITY OF CALIFORNIA

APPLIED SCIENCE
DIVISION

Technology Base Research Project for
Electrochemical Energy Storage

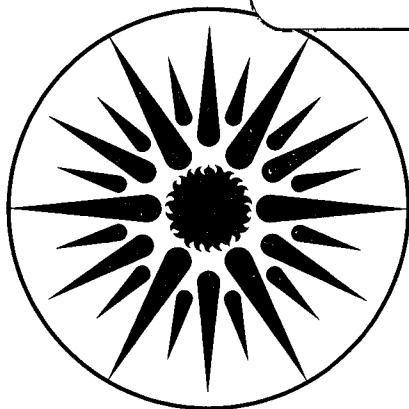
Annual Report for 1990

June 1991

U. C. Lawrence Berkeley Laboratory
Library, Berkeley

FOR REFERENCE

Not to be taken from this room



APPLIED SCIENCE
DIVISION

DISCLAIMER

This document was prepared as an account of work sponsored by the United States Government. While this document is believed to contain correct information, neither the United States Government nor any agency thereof, nor the Regents of the University of California, nor any of their employees, makes any warranty, express or implied, or assumes any legal responsibility for the accuracy, completeness, or usefulness of any information, apparatus, product, or process disclosed, or represents that its use would not infringe privately owned rights. Reference herein to any specific commercial product, process, or service by its trade name, trademark, manufacturer, or otherwise, does not necessarily constitute or imply its endorsement, recommendation, or favoring by the United States Government or any agency thereof, or the Regents of the University of California. The views and opinions of authors expressed herein do not necessarily state or reflect those of the United States Government or any agency thereof or the Regents of the University of California.

**TECHNOLOGY BASE RESEARCH PROJECT
FOR
ELECTROCHEMICAL ENERGY STORAGE**

**ANNUAL REPORT
FOR 1990**

Applied Science Division
Lawrence Berkeley Laboratory
1 Cyclotron Road
Berkeley, California 94720

Edited by Kim Kinoshita, Technical Manager

June 1991

This work was supported by the Assistant Secretary for Conservation and Renewable Energy, Office of Propulsion Systems, Energy & Hybrid Propulsion Division of the U.S. Department of Energy under Contract No. DE-AC03-76SF00098.

CONTENTS

EXECUTIVE SUMMARY	v
I. INTRODUCTION	1
II. EXPLORATORY RESEARCH	
A. ADVANCED ZINC/NICKEL OXIDE CELLS	
Zn/KOH/NiOOH Cell Studies	2
B. SOLID-STATE LITHIUM/REDOX POLYMERIZATION CELLS	
Electrochemical Properties of Lithium/Redox Polymerization Cells	3
C. MOLTEN-SALT CELLS	
Molten-Salt Li-Alloy/FeS ₂ Cell Research	4
III. APPLIED SCIENCE RESEARCH	
A. ALKALINE CELLS	
Zinc Electrode Studies	9
Surface Morphology of Metals in Electrodeposition	10
B. LEAD/ACID CELLS	
Battery Materials: Structure and Characterization	12
C. COMPONENTS FOR HIGH-TEMPERATURE CELLS	
High-Temperature Cell Research	13
Sodium/Metal Chloride Cell Research	14
New Battery Materials	16
D. CORROSION PROCESSES IN HIGH-SPECIFIC-ENERGY CELLS	
Corrosion-Resistant Coatings for High-Temperature	
High-Sulfur-Activity Applications	17
Corrosion, Passivity, and Breakdown of Alloys Used in High-Energy Batteries	18
E. COMPONENTS FOR AMBIENT-TEMPERATURE NONAQUEOUS CELLS	
Spectroscopic Studies of the Passive Film on Alkali and	
Alkaline Earth Metals in Nonaqueous Solvents: A Surface Science Approach	19
<i>In Situ</i> Raman Spectroscopy of Lithium Electrode Surfaces in Alkaline Cells	20
Polymeric Electrolytes for Ambient-Temperature Batteries	21
Solid Polymer Electrolytes for Rechargeable Batteries	21
F. CROSS-CUTTING RESEARCH	
Analysis and Simulation of Electrochemical Systems	22
Surface Layers on Battery Materials	23
Application of Photothermal Deflection Spectroscopy to Electrochemical Interfaces	24
Electrode Kinetics and Electrocatalysis of Methanol Electrooxidation	25
Engineering Analysis of Gas Evolution	26
IV. AIR SYSTEMS RESEARCH	
A. METAL/AIR CELL RESEARCH	
Electrocatalysts for Oxygen Electrodes	28
Electrical and Electrochemical Behavior of Particulate Electrodes	30
Zinc/Air Battery Development for Electric Vehicles	31
B. FUEL CELL RESEARCH	
Fuel Cells For Renewable Applications	31
Advanced Chemistry and Materials for Fuel Cells	35

EXECUTIVE SUMMARY

The U.S. Department of Energy's Office of Propulsion Systems provides support for an electrochemical energy storage program, which includes R&D on advanced rechargeable batteries and fuel cells. A major goal of this program is to develop electrochemical power sources suitable for application in electric vehicles (EVs). The program centers on advanced systems that offer the potential for high performance and low life-cycle costs, both of which are necessary to permit significant penetration into commercial markets.

The DOE Electrochemical Energy Storage Program is divided into two projects: the Exploratory Technology Development and Testing (ETD) Project and the Technology Base Research (TBR) Project. The ETD Project management responsibility has been assigned to Sandia National Laboratory (SNL), and the Lawrence Berkeley Laboratory* (LBL) is responsible for management of the TBR Project. The ETD and TBR Projects include an integrated matrix of research and development efforts designed to advance progress on several candidate electrochemical systems. The role of the TBR Project is to perform supporting research for the advanced battery systems under development by the ETD Project, and to evaluate new systems with potentially superior performance, durability and/or cost characteristics. The specific goal of the TBR Project is to identify the most promising electrochemical technologies and transfer them to industry and/or the ETD Project for further development and scale-up. This report summarizes the research, financial and management activities relevant to the TBR Project in CY 1990. This is a continuing project, and reports for prior years have been published; they are listed at the end of the Executive Summary.

The general R&D areas addressed by the project include identification of new electrochemical couples for advanced batteries, determination of technical feasibility of the new couples, improvements in battery components and materials, establishment of engineering principles applicable to electrochemical energy storage and conversion, and the development of air-system (fuel cell, metal/air) technology for transportation applications. Major emphasis is given to applied research which will lead to superior performance and lower life-cycle costs.

The TBR Project is divided into three major project elements: Exploratory Research, Applied Science Research, and Air Systems Research. Highlights of each project element are summarized according to the appropriate battery system or electrochemical research area.

* Participants in the TBR Project include the following LBL scientists: E. Cairns, K. Kinoshita and F. McLarnon of the Applied Science Division; and L. DeJonghe, J. Evans, R. Muller, J. Newman, P. Ross and C. Tobias of the Materials and Chemical Sciences Divisions.

EXPLORATORY RESEARCH

The objectives of this project element are to identify, evaluate and initiate development of new electrochemical couples with the potential to meet or exceed advanced battery and electrochemical performance goals. Research was conducted on new versions of the **Zn/NiOOH cell**, and a novel **Li/polymer/redox polymerization cell**. Each of these cells is considered to be an attractive candidate for EV applications, and may provide high performance at ambient or near-ambient temperatures. Research was also conducted on high-temperature **molten-salt cells** based on Li-alloy negative electrodes and metal disulfide positive electrodes. These cells exhibit very high performance, ease of manufacture, and freeze-thaw capability. Several key issues for this technology are to: *i*) stabilize the performance of the FeS_2 electrode, *ii*) develop corrosion-resistant containment materials, and *iii*) identify improved sealant materials.

- LBL has been able to virtually eliminate the major problems restricting the cycle-life performance of Zn/KOH/NiOOH cells. A sealed, maintenance-free cell has accumulated 400 deep-discharge cycles with almost no shape change, and a vented cell has accumulated more than 800 deep-discharge cycles with about 30% capacity loss. The shape-change problem was overcome by use of carbonate- or fluoride-containing electrolytes. Dendritic shorting and reformation problems were solved by the use of a sealed, electrolyte-starved cell configuration in which O_2 , generated during charge, scavenges incipient Zn dendrites that may be present.
- LBL has succeeded in cycling lithium/poly(ethylene) oxide/solid redox polymerization electrode (Li/PEO/SRPE) cells at lower temperatures than typically used with Li/polymer cells. The PEO electrolytes were modified so that they do not crystallize at lower temperatures, instead maintaining their amorphous character and reasonable ionic conductivity. At 20°C, the cells were cycled for greater than 100 cycles at a volumetric power density of 30 W/l. At elevated temperatures, 70-90°C, hundreds of cycles are readily achieved with an estimated specific power of 120 W/kg.
- Argonne National Laboratory (ANL) has developed new sealant materials (a mixed chalcogenide) which are electronic insulators and bond strongly to metals and ceramics, even after exposure to molten salt containing Li alloy or FeS_2 at 400-450°C. The mixed chalcogenide exhibited a bond strength that was about ten times stronger than that of commercially available bonding agents such as borosilicate glass and silane-based products.
- ANL has also fabricated a bipolar four-cell Li/ FeS_2 stack with the new sealant materials which operated for >500 cycles with >98% coulombic efficiency.

- A mathematical model was developed by ANL which was able to predict the self-discharge rates of Li/FeS₂ cells. This semi-empirical model incorporated parameters such as the Li diffusion coefficient, electronic conductivity of electrolyte, and Li activities at the positive and negative electrodes.

APPLIED SCIENCE RESEARCH

The objectives of this project element are to provide and establish scientific and engineering principles applicable to batteries and electrochemical systems; and to identify, characterize and improve materials and components for use in batteries and electrochemical systems. Projects in this element provide research that supports a wide range of battery systems - alkaline, metal/air, flow, solid-electrolyte, and nonaqueous. Other cross-cutting research efforts are directed at improving the understanding of electrochemical engineering principles, minimizing corrosion of battery components, analyzing the surfaces of electrodes, and electrocatalysis.

Alkaline Cells often use Zn as the negative electrode, and it is this electrode that typically limits the lifetime of these cells. Efforts are underway to identify electrode and electrolyte compositions that will improve the cycle-life performance of the Zn electrode, and to determine the operating conditions that lead to Zn dendrite formation.

- LBL has implemented a one-dimensional, time-dependent model of the Zn/NiOOH cell to characterize the transport of soluble Zn species from the Zn electrode to the NiOOH electrode. This model predicted that the greater the amount of Zn allowed to leave and reenter the NiOOH electrode, the faster the rate and extent of shape change, with Zn material moving from the center towards the edges of the Zn electrode.
- LBL has developed two-dimensional mathematical models of current and potential distributions and mass-transfer processes in model Zn pore electrodes. The results from these models were in good agreement with the experimental data for a model pore obtained by optical probe beam deflection.
- Videomicroscopic recordings at LBL of the Zn deposition process in a flow channel has revealed that moss formation is initiated only after a more or less substantial "compact" layer is formed, when large protrusions appear on the surface. The mossy Zn deposits are formed in alkaline electrolytes over a wide range of current densities and flow rates.

Lead/Acid Cells use positive electrodes of lead oxides which exist in different phase compositions and stoichiometry. The character of the positive active material, which is formed electro-

chemically, has a major influence on the performance and life of the lead/acid battery. Thus, understanding the properties of these lead oxides and their changing properties during charge-discharge would be helpful in promoting longer cycle life.

- Brookhaven National Laboratory (BNL) has used extended x-ray absorption fine structure (EXAFS) and x-ray absorption near-edge spectroscopy (XANES) to study the oxides of Pb. A marked difference was observed in the x-ray absorption spectra of α -PbO₂ and γ -PbO₂. The stoichiometry of PbO₂ in the formed battery electrode was lower than that found for electrochemically or chemically prepared γ -PbO₂.

Improved Components for Alkali/Sulfur and Alkali/Metal Chloride Cells, such as superior alternatives to the β "-Al₂O₃ ceramic electrolyte and the high-temperature sulfur-polysulfide electrode for Na/S cells, stable Li-ion conductors for Li/S cells, and optimized NiCl₂ electrodes for Na/NiCl₂ cells, are under investigation.

- ANL has developed a new fabrication technique which produced Ni electrodes for Na/NiCl₂ cells with higher and more uniform porosity. These electrodes had significantly lower impedance than the electrodes in the state-of-the-art cells.
- ANL has developed a technique to investigate the charging of Ni electrodes in Na/NiCl₂ cells. During charge NiCl₂ forms a poorly conducting layer on the surface of the Ni electrode, and increases the impedance. This layer increases in thickness and hinders further charge of the electrode.
- Stanford University has identified an intermediate phase (Na₆FeC₁₈) that forms during discharge of Na/FeCl₂ cells. In the case of Na/NiCl₂ cells, no intermediate phase forms during discharge. This study further concluded that the formation of eutectic compositions in the Na/FeCl₂ and Na/NiCl₂ cells at 370 and 570°C, respectively, limits their maximum operating temperatures to ~300 and ~500°C, respectively.

Corrosion Processes in High-Specific-Energy Cells are under investigation and the aim is to develop low-cost container and current-collector materials for use in nonaqueous, alkali/sulfur, and molten-salt cells.

- Illinois Institute of Technology (IIT) has successfully electrodeposited Mo₂C coatings on the internal surface of the cell casings for Na/S cells from Chloride Silent Power Ltd. (CSPL). In general, the test results at CSPL were encouraging but further optimization of coating quality is necessary for long-term endurance. Evaluation of electrodeposited Mo₂C-coated Ni in a Li/FeS₂ cell at ANL showed that these coatings are stable at 1 to 2.1 V (*vs* LiAl reference elec-

trode) for 57 h. Corrosion was evident at 2.2 V, which is attributed to the presence of pinholes in the coating.

- Johns Hopkins University has observed that Armco iron and 1018 carbon steel, which are scratched to mechanically disrupt the air-formed film, are rapidly repassivated in dimethoxyethane (DME)/LiAsF₆ containing 300-ppm water. The adsorption of DME molecules or the precipitation of an iron hexafluoroarsenate salt film is believed to be responsible for the rapid repassivation.

Components for Ambient-Temperature Nonaqueous Cells, particularly metal/electrolyte combinations that improve the rechargeability of these cells, are under investigation.

- Case Western Reserve University (CWRU) has used *in situ* Attenuated Total Reflection Fourier Transform Infrared Spectroscopy to study the lithium/poly(ethyleneoxide) interface. Spectral features were identified at about 1100 cm⁻¹ which suggested that ether-type bonds were cleaved and alkoxide functionalities (e.g., $-(CH_2)-O-Li^+$) were formed. This technique appears to be useful for investigating the chemical/electrochemical interactions at electrode/conducting polymer interfaces.
- The University of Pennsylvania has obtained encouraging results with Li-ion conducting polymers containing a plasticizer (propylene carbonate, polyethylene glycol dimethylether-Poly 500) and Li salts (LiClO₄, LiCF₃SO₃, LiAsF₆). The ionic conductivity of the polymer with Poly 500 was lower than that with PC, but its mechanical, thermal and transport properties were better. These electrolytes exhibited good electrochemical and mechanical properties in preliminary studies over 20-30 Li plating/stripping cycles in small cells.
- SRI International has developed a Li-ion conducting polysiloxane which has one of the highest ionic conductivities (1.8×10^{-4} ohm⁻¹ cm⁻¹ after exposure to MeCN) at room temperature reported so far.
- Jackson State University has observed by *in situ* Raman spectroscopy that Li is more reactive in diethyl carbonate (DEC) than in dimethyl carbonate. However, the addition of methyl formate to DEC suppressed the reactivity of Li.

Cross-Cutting Research is carried out to develop mathematical models of electrochemical systems, and to address fundamental problems in electrocatalysis and current-density distribution; solutions will lead to improved electrode structures and performance in batteries and fuel cells.

- LBL has developed mathematical models to understand transport and kinetic phenomena occurring in electrochemical systems. A model has been developed to predict the response to

alternating current of a redox species with soluble reactants and products in a flow-through porous electrode. Another model was developed which accounts for adsorption of chemical species on the electrode, the chemical or electrochemical reaction of the adsorbed species, and convective transfer during cyclic voltammetry.

- LBL employed laser Raman spectroscopy and cyclic voltammetry to investigate anodic Zn films in 1 M KOH. Evidence was obtained for the formation of a Zn(OH)₂ film during the active portion of the anodic potential sweep. Near the active-passive transition potential, the diffusion of hydroxide ions to the metal/film interface becomes rate limiting, and a film containing kinetically less-favored ZnO is formed.
- LBL is developing photothermal deflection spectroscopy (PDS) to study the electrooxidation of CH₃OH on Pt electrocatalyst. Preliminary studies of Pt electrooxidation suggest a two-reaction pathway whereby Pt(OH)₂ is formed by an electrochemical step and dehydrates by a chemical step to form PtO. This second step removes oxygen from the surface, which is just the opposite of what is needed for CH₃OH oxidation. This suggests that slowing the rate of dehydration could improve the overall reaction rate for CH₃OH electrooxidation.
- LBL has observed that the single-crystal face of the ordered alloy Pt₃Sn is not as good an electrocatalyst for methanol electrooxidation in sulfuric acid as a low-index single-crystal Pt with electrodeposited Sn.
- A novel system was designed at LBL to study the coalescence of small gas bubbles that are generated during electrochemical gas evolution. A high-speed, spatially resolved photodetector and data acquisition unit, with laser imaging, was used to follow the coalescence event. The coalescence of small gas bubbles (*e.g.*, 500-1000 μm) was observed.

AIR SYSTEMS RESEARCH

The objectives of this project element are to identify, characterize and improve materials for air electrodes; and to identify, evaluate and initiate development of metal/air battery systems and fuel-cell technology for transportation applications.

Metal/Air Cell Research projects address bifunctional air electrodes that are needed for electrically rechargeable metal/air (Zn/air, Fe/air) cells, and novel alkaline Zn electrode structures that could be used in either electrically recharged or mechanically recharged cell configurations.

- CWRU has observed that the pyrochlore, $\text{Pb}_2\text{Ru}_2\text{O}_{7-y}$, shows good activity for the reduction of O_2 in alkaline solution. The pyrochlore showed a higher activity than the perovskite metal oxide, $\text{SrFe}_x\text{Ru}_{1-x}\text{O}_{3-y}$, which also contains Ru. However, the perovskite may be useful as an electrocatalyst support because of its metallic conductivity.
- LBL has successfully demonstrated the mechanical evacuation/refilling of a Zn/air cell with a particulate Zn electrode and electrolyte. The regeneration of Zn particles from alkaline zincate solution was also demonstrated with an energy consumption of as low as 2.3 kWh/kg Zn.
- Metal Air Technology Systems International (MATSI) has discovered that a higher KOH concentration of 45 wt% is beneficial for obtaining high surface area and electroactive Zn deposits during charge of Zn/air cells with a reticulated Cu-foam structure for the Zn electrode. Two or three layers of Celgard 3401 were demonstrated to be sufficient to effectively eliminate the probability of cell shorting by Zn dendrites.

Fuel Cell Research, managed by Los Alamos National Laboratory (LANL), includes research in several areas of electrochemistry, theoretical studies, fuel-cell testing, fuel processing, and membrane characterization. Major achievements of the fuel-cell program during 1990 are listed below:

- LANL has developed a novel minicell which was used to investigate oxygen reduction at a Pt/recast Nafion interface. The rate of oxygen reduction decreased as the temperature was increased to 80°C, which was attributed to the loss of water from the Nafion film.
- LANL utilized ^1H NMR to measure the self-diffusion coefficient of protons in Nafion with different degrees of hydration. The results indicate that the diffusion coefficient decreases with a decrease in the water content.
- A one-dimensional model was developed by LANL to describe the complete proton exchange membrane (PEM) fuel cell. The model shows that the electroosmotic water drag causes a local depletion of water near the anode, which becomes more severe at higher current densities.
- A new test stand was designed and built at LANL. A single cell was operated for over 2100 h before it was voluntarily terminated because of equipment failure.
- International Fuel Cells, which has a subcontract with LANL, tested PEM fuel cells with low Pt loadings. They were able to duplicate the results obtained at LANL in small 5 cm × 5 cm

cells, and they showed that an alternate membrane ("Membrane C") gave performance comparable to other experimental membranes.

- BNL has investigated underpotential deposited (UPD) Sn on Pt as an electrocatalyst for methanol oxidation. EXAFS studies indicate the presence of Sn-O interactions, which vary in a continuous and reversible fashion with potential. These interactions are most probably the reason for the observation that UPD Sn on Pt is a good catalyst for the direct oxidation of methanol.

MILESTONES FOR THE TECHNOLOGY BASE RESEARCH PROJECT

Milestones accomplished in Fiscal Year 1990 by the TBR Project include:

- "Go/no-go decision on the use of non-Pt electrocatalysts in PEM fuel cells"

This study indicates that the currently available organo-metallic macrocycles (FeTMPP, CoTMPP) are not sufficiently electrocatalytically active to serve as a substitute for Pt. The best results for oxygen reduction were obtained with 1.65 mg/cm² CoTMPP, but this was still not as good as that obtained with 0.4 mg/cm² Pt.

- "Determine the effect of impurities such as sulfur and fluoride ions on the performance of MCl₂ electrodes"

A small addition (2 wt%) of sulfur or fluoride ions enhances the utilization of active material and reduces the area-specific resistance in the NiCl₂ electrode. When the content of the additive was increased to 20 wt%, no significant increase in performance was observed.

- "Demonstrate a new cell design for Zn/air cells that has a particulate Zn electrode and circulating electrolyte"

Small laboratory-scale Zn/air cells (80 cm² and 400 cm² air electrode area) have been tested. Natural convection of alkaline electrolyte was observed to occur in the cell with a particulate Zn electrode. The results of this study were published in *J. Appl. Electrochem.*, **21(2)**, 105 (1991).

- "Initiate R&D on novel methods for *in situ* characterization of electrode surfaces"

PDS has been adapted at LBL for the *in situ* characterization of Pt and Zn electrodes in electrochemical cells. The results of these studies are described in an LBL report (LBL-27081, April 1989), and a monograph to be published by John Wiley.

- “Demonstrate high performance in PEM fuel cells with lower Pt loadings, equivalent to 0.5-g Pt/kW”

The LANL study indicates that 0.8 W/cm² can be obtained in a PEM fuel cell with a 5-mil thick membrane and only 0.4-g Pt/kW.

- “Complete EXAFS study of Zn electrolyte complexes”

EXAFS analysis of dissolved ZnO in alkali solution indicates the presence of Zn(OH)₄⁼ ions with a Zn-O bond length of 1.97 Å. In 0.1 M ZnBr₂, the Zn⁺⁺ ions are mostly coordinated to water. However, with increasing concentration there is an increase in coordination with Br⁻ ions, until Zn-O complexes are completely eliminated and only ZnBr₄⁼ ions are observed.

- “Complete EXAFS study of carbon-supported pyrolyzed macrocycle electrocatalyst for oxygen reduction”

The experimental data for both pyrolyzed FeTMPP and CoTMPP suggest that the metal atom is coordinated to four nitrogen atoms in much the same way as that for the original macrocycle. Furthermore, this study concluded that the monodispersed Fe and Co atoms are the electrocatalysis sites.

- “Complete development of a time-dependent, one-dimensional mathematical model of the Zn/NiOOH cell”

The LBL model suggests that the non-uniformity of the current density, particularly the differences between charge and discharge, contributes to shape change of the Zn electrode. Furthermore, the different rates of chemical precipitation/dissolution alone cannot account for the process of shape change.

- “Complete development of improved design for advanced Na/MCl₂ cells”

Cell modeling studies indicated that higher surface area of solid electrolyte and thinner metal chloride electrodes are needed to achieve high-performance cells. It is suggested that a multi-tube design consisting of many long, small-diameter cells should be capable of producing higher performance.

- “Complete development and test of peripheral metal/ceramic seals for Li-alloy/FeS₂ cells”

A modified-chalcogenide sealant material showed improved wetting and better contact with Mo. A four-cell Li/FeS₂ stack with this new sealant material completed more than 500 cycles (2500 h) of operation with >98% coulombic efficiency.

- “Complete life test at high current density of a single PEM cell with low Pt loading”

The LANL test showed that no performance degradation was observed with 0.45 mg/cm² Pt loading in over 1200 h of continuous operation at 0.60-0.75 A/cm².

MANAGEMENT ACTIVITIES

During 1990, LBL managed 15 subcontracts and conducted a vigorous research program in Electrochemical Energy Storage. LBL staff members attended project review meetings, made site visits to subcontractors, and participated in technical management of various TBR projects. LBL staff members also participated in the following reviews, meetings, and workshops:

- IECEC Planning Meetings, Reno, NV, January 24-25, 1990
- DOE/EPRI Workshop to Identify Battery Requirements for Low-Maintenance Lead-Acid Battery Storage, EPRI, Palo Alto, CA, February 7-8, 1990
- Lead Center Coordination Meeting, LBL, Berkeley, CA, February 12, 1990
- Zinc Battery R&D Review Meeting, LBL, Berkeley, CA, February 13-15, 1990
- SNL Zinc/Bromine Battery Review Meeting, SNL, Albuquerque, NM, February 26-27, 1990
- Al/Air Battery Review Meeting, Washington, D.C., April 17, 1990
- 177th Meeting of the Electrochemical Society, Montreal, Canada, May 6-11, 1990
- Direct Methanol/Air Fuel Cell Workshop, Washington, D.C., May 14-16, 1990
- Alkaline Zinc Battery Meeting, LBL, Berkeley, CA, May 21-22, 1990
- PEM Fuel Cell Meeting, Washington, D.C., June 22, 1990
- 34th International Power Sources Symposium, Cherry Hill, NJ, June 25-28, 1990
- EPRI Solid Oxide Electrochemistry Workshop, Palo Alto, CA, July 11, 1990
- 25th IECEC Meeting, Reno, NV, August 12-17, 1990
- 41st Meeting of the International Society of Electrochemistry, Prague, Czechoslovakia, August 19-24, 1990
- International Battery Association Meeting, Tokyo, Japan, August 29-30, 1990
- Lead Center Meeting, ANL, Argonne, IL, September 5, 1990
- Electric Vehicle Project Review Meeting, ANL, Argonne, IL, September 6-7, 1990
- Workshop on Rechargeable Lithium Polymer Batteries, Kirkland, WA, October 11-13, 1990
- 178th Meeting of the Electrochemical Society, Seattle, WA, October 14-19, 1990
- Annual Meeting of the AIChE, Chicago, IL, November 11-16, 1990
- Fuel Cell Seminar, Phoenix, AZ, November 25-28, 1990

ACKNOWLEDGEMENT

This work was supported by the Assistant Secretary for Conservation and Renewable Energy, Office of Propulsion Systems, Energy & Hybrid Propulsion Division of the U.S. Department of Energy under Contract No. DE-AC03-76SF00098. The support from DOE and the contributions to this project by the participants in the TBR Project are acknowledged. The assistance of Ms. Susan Lauer for coordinating the publication of this report and Mr. Garth Burns for providing the financial data are gratefully acknowledged.

ANNUAL REPORTS

1. "Technology Base Research Project for Electrochemical Energy Storage - Annual Report for 1989," LBL-29155 (May 1990).
2. "Technology Base Research Project for Electrochemical Energy Storage - Annual Report for 1988," LBL-27037 (May 1989).
3. "Technology Base Research Project for Electrochemical Energy Storage - Annual Report for 1987," LBL-25507 (July 1988).
4. "Technology Base Research Project for Electrochemical Energy Storage - Annual Report for 1986," LBL-23495 (July 1987).
5. "Technology Base Research Project for Electrochemical Energy Storage - Annual Report for 1985," LBL-21342 (July 1986).
6. "Technology Base Research Project for Electrochemical Energy Storage - Annual Report for 1984," LBL-19545 (May 1985).
7. "Annual Report for 1983 - Technology Base Research Project for Electrochemical Energy Storage," LBL-17742 (May 1984).
8. "Technology Base Research Project for Electrochemical Energy Storage - Report for 1982" LBL-15992 (May 1983).
9. "Technology Base Research Project for Electrochemical Energy Storage - Report for 1981," LBL-14305 (June 1982).
10. "Applied Battery and Electrochemical Research Program Report for 1981," LBL-14304 (June 1982).
11. "Applied Battery and Electrochemical Research Program Report for Fiscal Year 1980," LBL-12514 (April 1981).

SUBCONTRACTOR FINANCIAL DATA - CY 1990

Subcontractor	Principal Investigator	Project	Contract Value (K\$)	Status Term (months)	Expiration Date	in CY 1990*
<i><u>EXPLORATORY RESEARCH</u></i>						
Molten-Salt Cells						
Argonne National Laboratory	C. Christianson	Molten-Salt Cells	275	12	9-90	C
<i><u>APPLIED SCIENCE RESEARCH</u></i>						
Lawrence Berkeley Laboratory	E. Cairns, L. DeJonghe, J. Evans, R. Muller, J. Newman, P. Ross, and C. Tobias	Electrochemical Energy Storage	1800	12	9-90	C
Acid Cells						
Brookhaven National Laboratory	J. McBreen	Zn Morphology	100	12	9-90	C
Components for High-Temperature Cells						
Argonne National Laboratory	C. Christianson	Solid Electrolytes	225	12	9-90	C
Stanford University	R. Huggins	New Battery Materials	100	6	5-91	T

Subcontractor	Principal Investigator	Project	Contract Value (K\$)	Status Term (months)	Expiration Date	in CY 1990*
<u>APPLIED SCIENCE RESEARCH - cont.</u>						
Corrosion Processes in High-Specific Energy Cells						
Illinois Institute of Technology	R. Selman	Corrosion Resistant Coatings	132	12	2-91	C
Johns Hopkins University	J. Kruger	Corrosion/Passivity Studies	90	12	8-91	C
Components for Ambient-Temperature Nonaqueous Cells						
Case Western Reserve University	D. Scherson	Spectroscopic Studies	51	12	4-91	C
Jackson State University	H. Tachikawa	Raman Spectroscopy	47	12	6-91	C
University of Pennsylvania	G. Farrington	Polymeric Electrolytes	47	12	5-91	C
SRI International	S. Narang	Polymeric Electrolytes	97	1	9-91	C
<u>AIR SYSTEMS RESEARCH</u>						
Metal/Air Cell Research						
Case Western Reserve University	E. Yeager	Air Electrodes	196	12	4-91	C
Metal Air Technology Systems	R. Putt	Zn/Air Battery	149	16	5-91	T
Fuel Cell R&D						
Los Alamos National Laboratory	S. Gottesfeld	Fuel Cell R&D	1300	12	9-90	C
Brookhaven National Laboratory	J. McBreen	Fuel Cell Research	100	12	9-90	C

* C = continuing, T = terminating

LIST OF ACRONYMS

AES	Auger electron spectroscopy
AIChE	American Institute of Chemical Engineers
ASI	area specific impedance
AN	acetonitrile
ANL	Argonne National Laboratory
ATRFTIRRAS	attenuated total reflection Fourier transform infrared reflectance absorption spectroscopy
BNL	Brookhaven National Laboratory
CSPL	Chloride Silent Power Limited
CTE	coefficient of thermal expansion
CVD	chemical vapor deposition
CWRU	Case Western Reserve University
DEC	diethyl carbonate
DHE	dynamic hydrogen electrode
DMC	dimethyl carbonate
DME	dimethoxyethane
DOD	depth of discharge
DOE	U.S. Department of Energy
DSC	differential scanning calorimetry
EMF	electromotive force
EPRI	Electric Power Research Institute
ETD	Exploratory Technology Development and Testing
EV	electric vehicle
EXAFS	extended x-ray absorption fine structure
FTIRRAS	Fourier transform infrared reflectance absorption spectroscopy
HOPG	highly ordered pyrolytic graphite
IAD	implicit alternating direction
ID	inner diameter
IECEC	Intersociety Energy Conversion Engineering Conference
IFC	International Fuel Cells, Inc.
IIT	Illinois Institute of Technology
ISE	International Society of Electrochemistry
LANL	Los Alamos National Laboratory
LBL	Lawrence Berkeley Laboratory
LEED	low energy electron diffraction
LEISS	low energy ion scattering spectroscopy
M&EA	membrane/electrode assemblies
MA	methyl acetate
MATSI	Metal Air Technology Systems International

MF	methyl formate
MSECD	Molten Salt Electrochemical Deposition
NMR	nuclear magnetic resonance
OPG	ordinary pyrolytic graphite
PC	propylene carbonate
PDE	partial differential equation
PDS	photothermal deflection spectroscopy
PECVD	plasma-enhanced chemical vapor deposition
PEM	proton-exchange membrane
PEO	poly(ethylene oxide)
PGSE	pulsed-field-gradient, spin-echo NMR
PTFE	polytetrafluoroethylene
RF	radio frequency
SCE	saturated calomel electrode
SEM	scanning electron microscopy
SFUDS	simplified federal urban driving schedule
SNL	Sandia National Laboratories
SRPE	solid redox polymerization electrode
SPE	solid polymer electrolyte
STM	scanning tunneling microscopy
TBR	Technology Base Research
TEM	transmission electron microscopy
TMPP	tetramethoxyphenyl porphyrin
TSPP	tetra kis(sulfonated) porphyrin
TTAPP	tetra kis(4-trimethyl ammonium phenyl) porphyrin
UHV	ultrahigh vacuum
UPD	underpotential deposition
VLSI	very large-scale integration
XANES	x-ray near edge absorption spectroscopy
XAS	x-ray absorption spectra
XRD	x-ray diffraction
XRM	x-ray microanalysis

I. INTRODUCTION

This report summarizes the progress made by the Technology Base Research (TBR) Project for Electrochemical Energy Storage during calendar year 1990. The primary objective of the TBR Project, which is sponsored by the U.S. Department of Energy (DOE) and managed by Lawrence Berkeley Laboratory (LBL), is to identify electrochemical technologies that can satisfy stringent performance and economic requirements for electric vehicles and stationary energy storage applications. The ultimate goal is to transfer the most-promising electrochemical technologies to the private sector or to another DOE project (*e.g.*, SNL's ETD Project) for further development and scale-up.

Besides LBL, which has overall responsibility for the TBR Project, LANL, BNL and ANL have partici-

pated in the TBR Project by providing key research support in several of the project elements.

The TBR Project consists of three major elements:

- Exploratory Research
- Applied Science Research
- Air Systems Research

The objectives and the specific battery and electrochemical systems addressed by each project element are discussed in the following sections, which also include technical summaries that relate to the individual projects. Financial information that relates to the various projects and a description of the management activities for the TBR Project are described in the Executive Summary.

II. EXPLORATORY RESEARCH

The major thrust of this project element is to evaluate promising electrochemical couples for advanced batteries for electric vehicles. The only advanced large-size electrochemical system that was investigated is based on a high-temperature Li molten salt cell. Exploratory research was carried out on Zn/NiOOH and Li/polymer/redox polymerization cells. Novel components for various versions of rechargeable Li, Na, and Zn cells were also investigated, as described in the Applied Science section of this report.

A. ADVANCED ZINC/NICKEL OXIDE CELLS

New approaches to extend the cycle life of Zn/NiOOH cells are underway that involve modifying the electrolyte composition.

Zn/KOH/NiOOH Cell Studies

E.J. Cairns and F.R. McLarnon (Lawrence Berkeley Laboratory)

The purpose of this research is to study the life- and performance-limiting phenomena of Zn/NiOOH cells under realistic operating conditions. The major problems (*i.e.*, shape-change, Zn dendrites) restricting the cycle-life performance of 1.35-Ah Zn/KOH/NiOOH cells have now been mitigated to a major extent. The shape-change problem has been significantly reduced by the use of electrolyte compositions having low zincate solubility. In flooded, vented cells cycled at 100% depth-of-discharge (DOD), a cell with 2.5 M KOH-2.5 M K_2CO_3 -0.5 M LiOH electrolyte retained 60% of its initial capacity after 470 cycles, and a cell with 3.5 M KOH-3.3 M KF electrolyte retained 70% of its initial capacity after 820 cycles (Figure 1). *In situ* x-ray photographs of these cells revealed only moderate Zn redistribution, but the cells occasionally experienced minor dendritic shorts. These cells exhibited peak specific powers ranging from 200 to 300 W/kg, which is more than adequate for electric vehicle (EV) applications. Dendritic shorting and reformation problems were solved by the use of a sealed, electrolyte-starved cell configuration in which the cell is sealed under vacuum, and the quantity of electrolyte is limited to fill the pores of the electrodes and

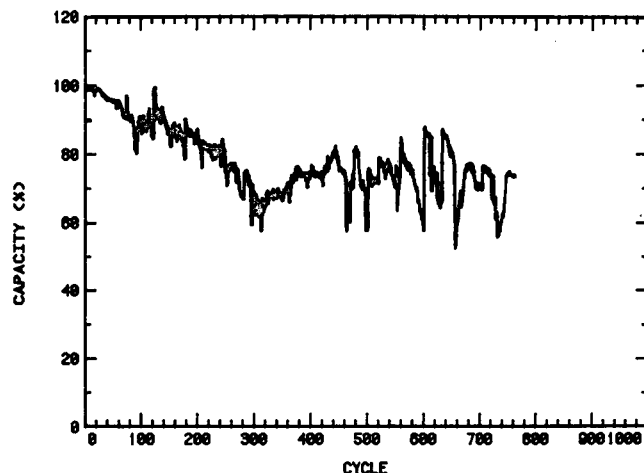


Figure 1. Capacity vs cycle number (100% DOD) for cell containing 3.5 M KOH - 3.3 M KF. (XBL 917-1419)

separator materials. As the cell is cycled the inefficiency of the NiOOH electrode produces an O_2 -enriched atmosphere in the cell. The O_2 not only reacts with the Zn metal in the negative electrode, thereby eliminating the need for reformation, but also scavenges incipient Zn dendrites. In this sealed, electrolyte-starved configuration, a 6.8 M KOH-0.5 M LiOH standard electrolyte cell reached 190 deep-discharge cycles, which is a 50% improvement over flooded, vented control cells. Another sealed, electrolyte-starved cell with low Zn-solubility electrolyte retained 80% of its original capacity after 400 deep-discharge cycles, and exhibits almost no shape-change. Both of these cells were essentially maintenance-free, showed no dendrites, and required no reformation cycles. These characteristics are ideal for EV and other applications.

B. SOLID-STATE LITHIUM/REDOX POLYMERIZATION CELLS

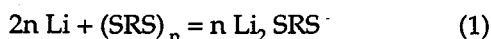
A novel Li/polymer cell has been developed which utilizes a solid redox polymerization electrode (SRPE). The cathode is a simple organodisulfide compound which is capable of undergoing repetitive charge-discharge cycling.

Electrochemical Properties of Lithium/Redox Polymerization Cells

L.C. DeJonghe (Lawrence Berkeley Laboratory)

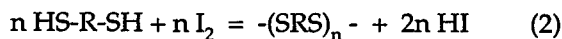
The objective of this research program is to develop advanced secondary batteries based on SRPEs. These materials show extremely encouraging results as potential candidates for EV applications. All-solid-state Li/PEO/SRPE cells were constructed using thin-film techniques and characterized in terms of specific energy and power, cycle life, and temperature dependence on cell performance. Fundamental studies of solid polymer electrolytes (SPEs) were also coupled with in-cell data in an effort to optimize cell performance.

The cell reaction for a simple linear organodisulfide polymer can be represented as



where R is an organic moiety such as CH_2CH_2 , C_2H_4 , etc. The cost projections for rechargeable high-performance batteries based on this technology are competitive with lead-acid batteries, yet this system offers far higher specific energy and volumetric energy density. Also, the non-toxic, biodegradable nature of the various components of Li/PEO/SRPE cells promises minimal recycling problems at the end of their service life.

A large number of organodisulfide polymers, $-(\text{SRS})_n-$, and copolymers $(\text{SRS})_x(\text{SR}'\text{S})_y$ were prepared and characterized. The polymers/copolymers were generally synthesized by oxidation of dithio and/or polythio acids by suitable oxidants as outlined below,



The oxido-polymerization reactions are carried out in aqueous solution and are often quite rapid, going to completion in a few minutes to a few hours. Copolymers are synthesized by simultaneously oxidizing a mixture of multi-thio acids having various R groups. The polymers are vacuum dried for several weeks prior to testing in solid-state cells.

Thin-film electrolytes and composite electrodes are cast from solution as described below. Anhydrous acetonitrile, chloroform, tetrahydrofuran, and crystalline polyethylene oxide (PEO) of various molecular weights (3×10^5 to 5×10^6) are used for film casting. PEO-based electrolytes (10-100 μm) are cast from mixtures of a solution of PEO in acetonitrile (or other suitable solvent) and solutions of appropriate Li

or Na salts, depending on the alkali metal anode to be used in the cell. Thin films of the organic cathodes (6-15 mg/cm^2) with surface capacities of 1 to 6 C/cm^2 are cast from solutions of PEO and redox polymers (with or without electrolyte salts) in an appropriate solvent or mixed solvents with dispersed carbon black. Composition of the composite cathodes are varied as a function of loading (wt%) of active material, amount of carbon black, and in a matrix of PEO electrolyte. The thin films are dried under vacuum at 50°C for 2 days and subsequently kept under vacuum for a few weeks prior to testing.

"Battery grade" Li foil (thickness of 25-100 μm) is obtained from Lithco Co. and stored in an argon atmosphere dry box. All-solid-state, thin-film, alkali metal/SRPE cells are constructed by sandwiching a polymeric electrolyte between the thin-film composite SRPE cathode and a thin foil of alkali metal; the battery is positioned between matching stainless-steel-plate current collectors. The solid-state cells are then cycled at various current densities, with intermittent high-power pulse testing.

A number of new SRPEs were synthesized and evaluated in solid-state Li cells. These included polymers based on 2,4-dithiopyrimidine, 2-mercaptoethyl ether, 2-mercaptoethyl sulfide, and ethane dithiol. The poly(diethyl ether disulfide) polymer (termed X0) exhibited good discharge kinetics and was exceptionally easy to cast as a homogeneous film due to its solubility in acetonitrile. The oxidation product of ethane dithiol, polyethylene disulfide (termed X8), also exhibited excellent discharge characteristics in solid-state cells (Figure 2, for example), and attained the highest surface capacities seen to date for solid-state SPE cells. Composite cathodes based on X8

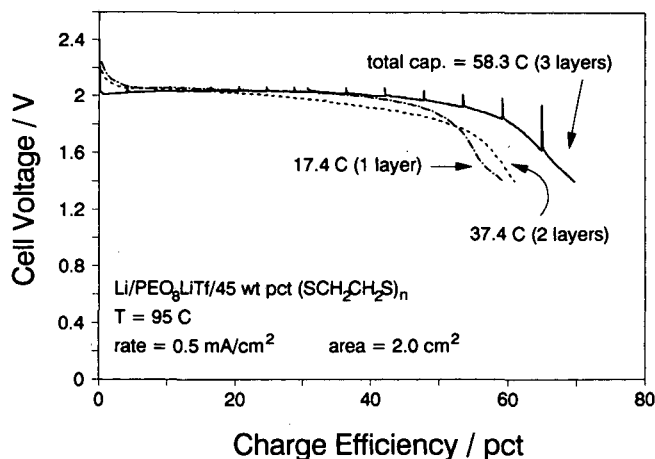


Figure 2. Discharge curves for X8 multilayer cathode. (XBL 917-1420)

showed no loss in utilization as a function of electrode thickness, and demonstrated cell capacities of greater than 20 C/cm² in Li/PEO/X8 cells operating at 80°C. Furthermore, polyethylene disulfide has an extremely low equivalent weight, 46 g/eq, and is a very inexpensive polymer to make in bulk. The low equivalent weight of X8 combined with the ability to attain high utilization with thick electrodes, makes possible solid-state cells with very high specific energy and volumetric energy density.

The possibility of synthesizing SRPE copolymers was successfully explored. A number of copolymers were produced and characterized in Li/PEO/(SRS)_x(SR'S)_y cells. The ability to produce copolymer electrodes serves a number of useful functions including overdischarge and overcharge protection by incorporating additional redox plateaus in the positive electrode polymers. Moreover, the physical/mechanical properties of the polymers can be modified in a beneficial way with copolymerization techniques.

Although the majority of Li/PEO/SRPE cells cycled in this laboratory were operated in the temperature range of 70 to 90°C, efforts in this program have succeeded in cycling all-solid-state cells at ambient temperature (20°C). In order to operate cells at 20°C, it was necessary to use modified PEO electrolytes which do not crystallize on cooling, but rather maintain their amorphous character and thereby are reasonably conductive at low temperatures. Ambient-temperature operation would probably not be desirable for EV applications because of the reduced power densities, however, these types of batteries have a tremendous advantage in that even if the battery pack were accidentally cooled to room temperature, sufficient current could be drawn from the battery to self-heat the cells, and possibly allow limited traction. At room temperature, Li/PEO/SRPE cells were cycled for greater than 100 cycles at a volumetric power density of 30 W/l, yet these cells could produce power densities of 230 W/l for one minute and pulse power of 500 W/l for a few seconds (figures based on the mass and volume of the laminate structure).

At elevated temperatures, 70-90°C, Li/PEO/SRPE cells (including mylar current collectors) are cycled at specific energy (volumetric) of 160 Wh/kg (190 Wh/l), and specific power (volumetric) of approximately 120 W/kg (140 W/l). Typically, hundreds of cycles are obtained, with the best to date approaching 350 cycles. In some cases, solid-state Li/PEO/SRPE cells demonstrated specific power of over 1 kW/kg with good electrode utilization.

PUBLICATIONS

1. M. Liu, S.J. Visco, and L.C. De Jonghe, "Electrode Kinetics of Organodisulfide Cathodes for Storage Batteries," *J. Electrochem. Soc.*, **137**, 750 (1990).
2. S.J. Visco, M. Liu, and L.C. De Jonghe, "Ambient Temperature High-Rate Lithium/Organosulfur Batteries," *J. Electrochem. Soc.*, **137**, 1191 (1990).
3. S.J. Visco, M. Liu, M.B. Armand, and L.C. DeJonghe, "Solid Redox Polymerization Electrodes and Their Use in All-Solid-State Batteries," *Mol. Cryst. Liq. Cryst.*, **190**, 185 (1990).

C. MOLTEN-SALT CELLS

Molten-Salt Cells based on Li-alloy negative electrodes and metal disulfide positive electrodes can exhibit very high performance, ease of manufacture, and freeze-thaw capability.

Molten-Salt Li-Alloy/FeS₂ Cell Research

D.R. Vissers (Argonne National Laboratory)

This research effort is focused on development of overcharge-tolerant monopolar and bipolar cells having molten-salt electrolyte, lithium-alloy negative electrodes, and metal disulfide positive electrodes. These cells are normally operated at temperatures of 375-425°C. In the bipolar cell, the positive and negative electrodes have a common current collector, the bipolar plate. These cells have a potential for high performance (200 Wh/kg and 500 W/kg), excellent cycle life (>1000 cycles), and low-cost fabrication. Accomplishments in 1990 included *i*) a 500-cycle test of a 4-cell stack of sealed bipolar Li/FeS₂ cells with overcharge tolerance, *ii*) development and demonstration of ceramic peripheral seals in bipolar cells having improved strength, and *iii*) a fundamental description of the overcharge tolerance mechanism in molten-salt Li cells.

The earlier studies indicated that a bipolar Li/FeS₂ battery has the potential for very high performance. In the bipolar cell, a hermetic seal is formed at the periphery prior to cell assembly. Here, a ceramic ring is sealed to Mo on one side to form the FeS₂ electrode housing, and a steel assembly is sealed to the other side of the ring to form the Li-alloy electrode housing. New sealant materials (mixed chalcogenides) were developed which are electronic insulators and bond tenaciously to metals and ceramics,

even after exposure to molten salt containing Li alloy or FeS_2 at 400-450°C. To date, over 24 seals have been fabricated and evaluated in bipolar Li/ FeS_2 cells. A seal with a graded coefficient of thermal expansion (CTE) that approximately matches the CTEs for both steel and Mo housings was developed, and six improved seals for the bipolar cell with similar ceramic compositions and processing methods were prepared. One seal was successfully leak-checked at a vacuum of 100 μm , the vacuum limit of the test fixture. Another seal was used to build a sealed bipolar Li/ FeS_2 cell (3-cm dia), which operated over 450 cycles and 2000 h and retained >90% of its initial capacity. The area-specific impedance (ASI) for this small-scale cell was 0.55 ohm-cm², which indicates the potential for high power with this technology. The remaining four seals were used to fabricate sealed bipolar Li/ FeS_2 cells for a four-cell stack.

The four-cell stack was operated for >500 cycles (2500 h) with >98% coulombic efficiency, as shown in Figure 3. Three of the four cells were employed throughout the tests, while one initially weak cell was replaced after 150 cycles. The bipolar stack capacity (0.45 Ah) was at least 90% that of individual cells. The stack was operated with charge and discharge cutoff voltages of 8.2 and 5.4 V, respectively. As shown in Figure 4, the bipolar Li/ FeS_2 stack at cycles 100 and 101 was operated at the 4-h charge and 2-h discharge rates. Voltages for the individual cells were well matched during these two cycles without the need for cell-to-cell charge equalization. During the stack lifetime, the voltage and capacity of individual cells with repeated recharging were sufficiently well matched that charge equalization was needed only every 20th cycle rather than every cycle. Charge equalization was achieved without electronic equip-

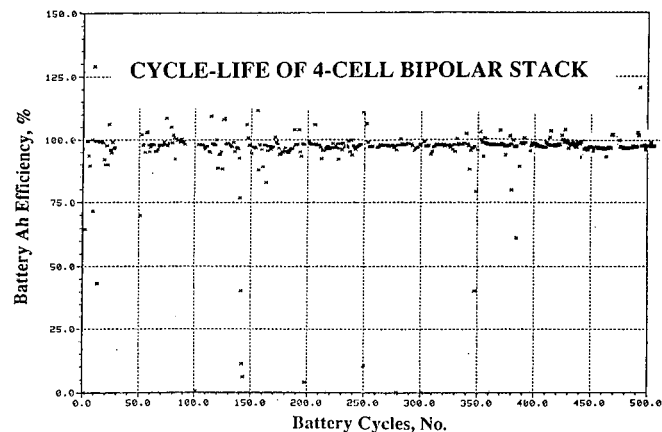


Figure 3. Coulombic efficiency of four-cell bipolar Li/ Fe_2 stack during 500 cycles of operation. (XBL 917-1421)

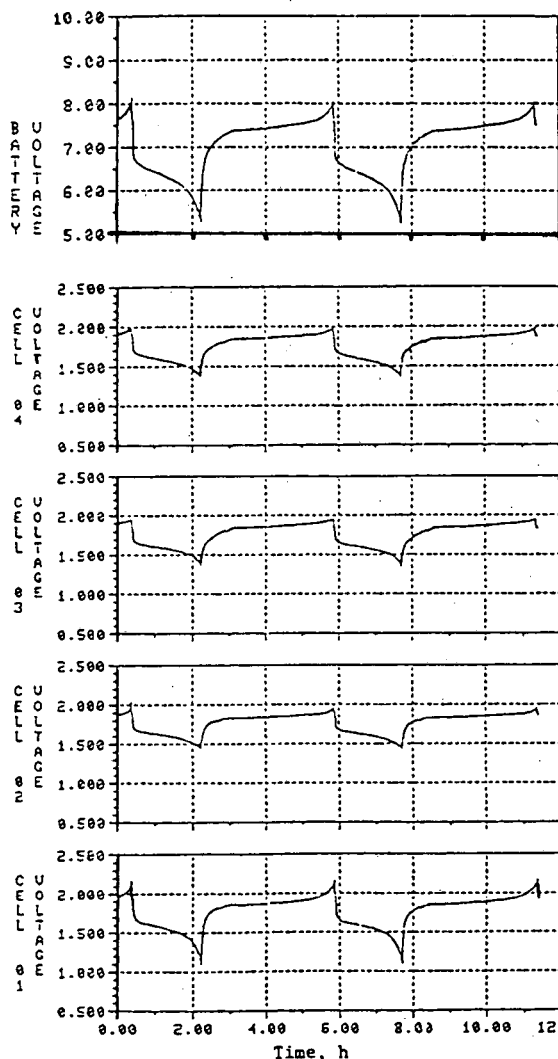


Figure 4. Voltage (in volts) of bipolar Li/ Fe_2 battery stack and individual cells vs time at cycles 100 and 101. (XBL 917-1422)

ment by use of an overcharge-tolerance mechanism for molten-salt cells, "the lithium-shuttle mechanism." By cell design, Li transport near the end of charge safeguards strong cells from overcharging, whereas weaker cells continue to accept charge.

An apparatus was developed to test the fracture strength of our composite ceramics used in the bipolar ring seal. The test determines the relative strengths of the various compositions that were developed. To date a six-fold increase in fracture strength was achieved by changing the filler-material composition of the ceramic. The baseline ceramic uses a CaO filler. The fracture strength of an Al_2O_3 filler sample was increased three-fold, while a new filler sample, $\text{B}_2\text{O}_3\text{-Al}_2\text{O}_3$ (90:10 mol%), produced a six-fold increase over the baseline ceramic.

The bond strength of ceramic/ceramic and metal/ceramic seals was determined to evaluate the effectiveness of the ceramic sealant materials. These physical data will provide a basis for developing the 130-mm ID peripheral seal needed for a prototype Li/FeS₂ bipolar battery. Test samples are prepared from two strips with 0.5- to 2.0-cm² bond areas. The bonded strips are mounted in a fixture that measures the shear force required to rupture the bond. There are no generally accepted test procedures of this type; therefore, the measurements are relative values. In these studies, over two dozen bond couples were formed and their sheer strength tested.

As shown in Table 1, bond strengths with the standard mixed-chalcogenide sealant are outstanding. Many times the substrate ruptures before the ceramic bond. For the Mo bond, the strength is improved by more than seven times by forming an intermetallic compound at the Mo surface prior to bond formation. In comparison to commercially available bonding agents for high-temperature application (e.g., borosilicate glass, silane-based Aremco products), the mixed-chalcogenide sealant materials exhibit bond strengths approximately ten times greater. Because the chalcogenides have excellent wetting properties, bond formation does not rely on a thermal/compression process; thus, the bonding is not unidirectional.

The stability of this high-strength ceramic with the B₂O₃·Al₂O₃ filler in the cell environment has been found to be excellent. A LiAl + LiAlFe/FeS₂ pellet cell, for example, was operated with a peripheral ring of this material and exhibited excellent performance and stability after 50 cycles of operation at 415°C. The utilization of the Li-alloy electrode was >80% of the theoretical capacity.

Another objective of the hermetic-seal development program is formation and testing of feedthrough seals for monopolar cells. Two feedthroughs having a 0.6-cm-diameter steel terminal were constructed from parts of the feedthrough used in the MK1A Battery Program of Eagle-Picher Industries, Inc. A swaged-type feedthrough body and terminal (both of steel) were set together with Al₂O₃ ring and MgO ceramic pieces. A hermetic seal was formed by bonding these components together with the sealant materials. The seals were tested by vacuum-leak checking at room temperature and 400°C, thermal cycling over a 1/2 hour period, and potentiometric stability testing at 1.6 V (half-cell testing). One feedthrough component maintained its leak tightness at 400°C in a half-cell test of >150 h.

Alternative electrolyte/separator materials were also tested in Li/FeS₂ cells. Initially, a bipolar Li/FeS₂ pellet cell with a salt-impregnated BN-felt separator

Table 1. Tensile Strength of Bonded Surfaces

Bond Couple	Surface Area (cm ²)	Load to Fracture (kg/cm ²)	Comment
Mo/standard sealant/Mo	2.0	3.2	
Mo/standard sealant/Mo (Mo intermetallic used)	0.5	23.0	Much improved
Mo/borosilicate glass/Mo	0.5	3.47	
Mo/standard sealant/graffoil (Mo intermetallic)	0.5	3.55	Grafoil tore before rupture
Al ₂ O ₃ /standard sealant/Al ₂ O ₃	0.72	19.76	
MgO/standard sealant/MgO	0.4	52.87	
Steel/standard sealant/MgO	0.48	>35.6	MgO fractured before bond
TiN-coated steel/standard sealant/TiN-coated steel	0.5	>16.7	Substrate tore before bond
Steel/Aremco 565/MgO	1.5	1.4	Other Aremco bonding agents failed before load test

was found to perform comparably with a similar cell having a MgO-powder separator. However, the capacity dropped by 30% at cycle 150 due to an increasing cell impedance, which may have been caused by electrolyte dewetting of the BN separator. Tests of Li/FeS₂ pellet cells using a "super-starved" separator (35 wt% electrolyte and 65% MgO) indicated that this separator severely reduced capacity (~10% lower utilization) and increased impedance by approximately fivefold.

Extensive measurements of Li transport rates using a potentiostated Li-AlFe electrode have provided the data needed for modeling overcharge tolerance in Li/FeS₂ cells. These Li transport rates were fit to Arrhenius-type expressions, as shown by the log Li shuttle rate vs reciprocal temperature plot (Figure 5) for three molten-salt electrolyte compositions. The proposed Arrhenius rate expressions agree well with available physical data for Li solubility and the complexing of Li in each of the three molten salts. It is assumed that Li₂⁺ is formed in the all-Li⁺ ion electrolyte (LiF-LiCl-LiBr), and that LiK⁺ is formed in the K⁺ ion-containing molten salts (LiCl-KCl, LiCl-LiBr-KBr).

Based on these fundamental considerations, a model of the overcharge tolerance mechanism has been formulated. The electronic conductivity of dissolved Li in the molten salt can be thought to short-circuit Li transport near the positive electrode, while the dimerization effectively removes electronic conductivity at the negative electrode side of the electro-

lyte layer. These concepts suggest a rather complicated model of the overcharge tolerance mechanism, with the Li diffusion constant, D, and electronic conductivity coefficient of electrolyte, k, varying across the thickness of the molten-salt electrolyte layer. Measurement of D and k would be difficult due to their interrelationship.

A semi-empirical model was developed for the overcharge tolerance (self-discharge) rate. An expression containing the Li diffusion and the electronic conductivity, as well as the Li activities at the respective electrodes, was derived:

$$i_s = A \ln \frac{a_2 + a_0}{a_1 + a_0} + BT[(a_2^n - a_1^n) - C(a_2 - a_1)] \quad (3)$$

where i_s = self-discharge rate, A/cm²
 a_2 = Li activity at the negative electrode
 a_1 = Li activity at the positive electrode
 a_0 = constant
 T = temperature, °K

The coefficients are defined as follows:

$$A = \frac{D}{t}, B = \frac{Rk_0}{Fnt}, C = \frac{nk_1}{k_0}, k = k_0 a^n - k_1 a \quad (4)$$

where D = diffusion coefficient of dissolved Li, expressed as A/cm
 t = distance between electrodes, cm
 R = ideal gas constant
 F = Faraday constant
 n = constant between zero and one (0.5 in these calculations)
 k = electronic conductivity of electrolyte
 k_0 and k_1 = coefficients in electronic conductivity equation

The measured self-discharge rates for the three electrolytes of interest (about 91 points) fit the model with excellent agreement. The ability to charge-equalize bipolar batteries without special electronics is a key development objective.

Studies on MgO separator technology were also conducted. The MgO powder separator, because it is not physically stable under flooded-electrolyte conditions, must be operated in the "electrolyte-starved" condition. The electrical resistivities of 20 electrolyte-starved MgO separator mixtures were measured by the DC-interruption technique which was developed for paste-like materials. These mixtures exhibited a large variation in resistivities and mechanical properties with salt composition, MgO concentration, and temperature. For example, Figure 6 shows the

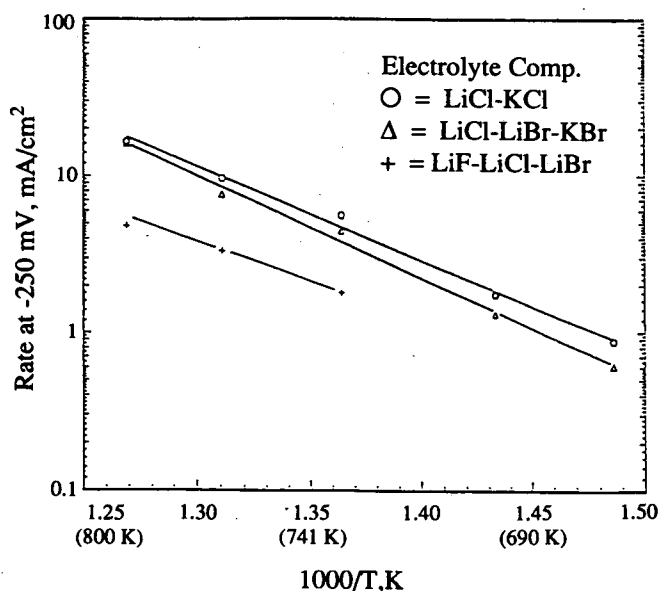


Figure 5. Effect of temperature upon Li shuttle rates at ~250 mV vs LiAl reference electrode.

(XBL 917-1423)

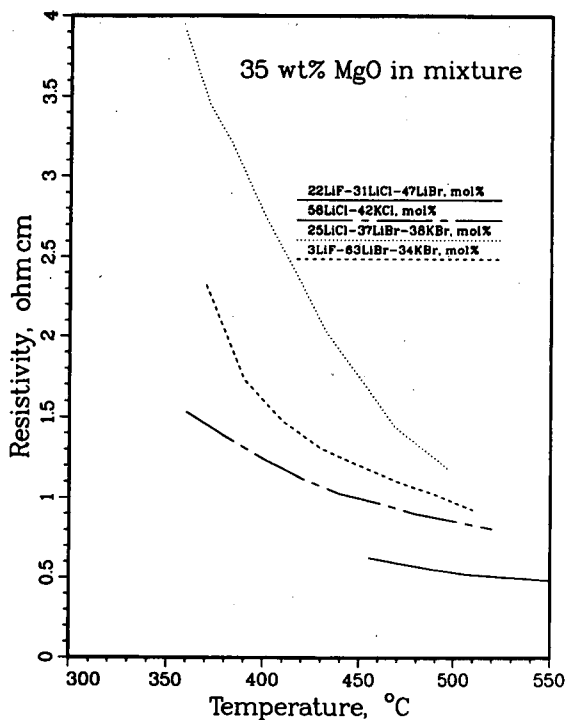


Figure 6. Effect of temperature on resistivities of MgO-salt mixtures prepared with 35 wt% MgO. (XBL 917-1424)

resistivities obtained for pellets of 35 wt% MgO mixed with salt of four different compositions as a function of temperature. The temperature effect is quite pronounced for three salt compositions, but relatively minor for the all-Li salt composition. The MgO content also influences the resistivity and mechanical properties of these electrolyte-starved separators. The magnitude of the impact differs for each salt composition, most likely due to differences in MgO wetting properties of the different salt mixtures.

A Mo₂C-coated Ni specimen prepared by Professor R. Selman of ITT (see Section III.D) was electrochemically characterized to study the corrosion resistance of Mo coatings for fabricating the cathode current collectors in Li/FeS₂ bipolar cells. The measurements involved cyclic voltammetry, constant-potential measurements, x-ray diffraction (XRD), and scanning electron microscopy (SEM). It was found that these coatings are chemically and electrochemically stable in the potential range of +1.0 to +2.1 V vs LiAl for at least 57 h. When the experiments were done at higher potential, +2.2 V vs LiAl, the coating corroded. Analyses with XRD and SEM showed that the corrosion was not due to a chemical reaction of the coating but rather to the presence of pinholes that opened up during the electrochemical measurements at +2.2 V vs LiAl.

PUBLICATIONS

1. L. Redey, "Overdischarge Protection in High-Temperature Cells and Batteries," *U.S. Patent No. 4,935,316* (June 19, 1990).
2. T.D. Kaun, M.J. Duoba, K.R. Gillie, M.C. Hash, D.R. Simon, and D.R. Vissers, "Development of a Sealed Bipolar Li-Alloy/FeS₂ Battery for Electric Vehicles," *Proc. of the 25th IECEC*, Reno, Nevada, Aug. 12-17, 1990, Vol. 3, p. 335.
3. T.D. Kaun, M.J. Duoba, K.R. Gillie, D.R. Simon, and D.R. Vissers, "Li-Alloy/FeS₂ as a Bipolar Battery," *34th Int'l. Power Sources Symp.*, Cherry Hill, NJ, June 25-28, 1990.
4. L. Redey, M. McParland, and R. Guidotti, "Resistivity Measurements of Halide Salt/MgO Separators for Thermal Cells," *34th Int'l. Power Sources Symp.*, Cherry Hill, NJ, June 25-28, 1990.

III. APPLIED SCIENCE RESEARCH

The objectives of this project element are to provide and establish scientific and engineering principles applicable to batteries and electrochemical systems; and to identify, characterize and improve materials and components for use in batteries and electrochemical systems. Projects in this element provide research that supports a wide range of battery systems - alkaline, flow, molten salt, nonaqueous, and solid-electrolyte. Other projects are directed at research on improving the understanding of electrochemical engineering principles, corrosion of battery components, surface analysis of electrodes, and electrocatalysis.

A. ALKALINE CELLS

Zinc is often used as the negative electrode in alkaline cells, and it is this electrode that typically limits the lifetime of these cells. Efforts are underway to identify cell components that will improve the cycle-life performance of the Zn electrode.

Zinc Electrode Studies

E.J. Cairns and F.R. McLarnon (Lawrence Berkeley Laboratory)

This research studies the behavior of Zn electrodes in secondary batteries and investigates practical means for improving their performance and lifetime using life- and performance-limiting phenomena under realistic cell operating conditions.

Mathematical Modeling. A one-dimensional, time-dependent model of the Zn/NiOOH cell was used to characterize the transport of soluble Zn species from the Zn electrode to the NiOOH electrode. Prior experiments showed that about 25% of the initial amount of Zn active material migrates from the Zn electrode to the Ni electrode during the first 2-3 cycles, however, the form in which the Zn exists is not well understood. The mathematical model accounted for this phenomenon by allowing 25% of the initial quantity of Zn to be incorporated in the NiOOH electrode, and then allowing 0-50% of that amount to leave the NiOOH electrode on charge and be redeposited on discharge. The 50% figure was selected after considering experimental observations, and deposition-dissolution was assumed to occur at a constant rate. It was found that the greater the

amount of Zn that was allowed to leave and reenter the NiOOH electrode, the faster the rate and extent of shape change, with Zn material moving from the center toward the edges of the Zn electrode.

Model Pore Studies. Mass transfer phenomena within a model pore, which is intended to simulate a microscopic pore existing in the electrode of a rechargeable Zn battery were investigated. The investigations employed optical probe-beam deflection as an *in situ* technique to measure electrolyte concentration gradients in a model pore. A two-dimensional mathematical model of the non-linear, secondary current and potential distributions within the model pore was developed. The numerical results of the model provided information about the reaction distribution along the model pore electrode, and helped determine how the active material in a porous electrode will be utilized during charge-discharge cycling. These calculations also provided the boundary conditions needed to calculate electrolyte concentration distributions in the model pore cell. A two-dimensional mathematical model of mass-transfer processes in the model pore cell was also developed. This mass-transfer model incorporates the abovementioned current-potential distribution model, and it allows direct, quantitative calculations of the concentrations of the electrolyte species. The results from the two mathematical models were in good quantitative agreement with the experimental data. The probe-beam deflection technique is therefore proven as a very useful technique for the investigation of mass transfer phenomena within a model pore. The good agreement between theory and experiment also suggests that the mathematical models adequately accounted for the physical and chemical processes occurring within an electrode pore.

PUBLICATIONS

1. M.J. Isaacson, F.R. McLarnon and E.J. Cairns, "Zinc Electrode Rest Potentials in Concentrated KOH-K₂Zn(OH)₄ Electrolytes," *J. Electrochem. Soc.*, **137**, 2361 (1990).
2. M.J. Isaacson, F.R. McLarnon and E.J. Cairns, "Current Density and ZnO Precipitation-Dissolution Distributions in Zn-ZnO Porous Electrodes and Their Effect on Material Redistribution: A Two-Dimensional Model," *J. Electrochem. Soc.*, **137**, 2014 (1990).

3. J. Weaver, F.R. McLarnon and E.J. Cairns, "Experimental and Theoretical Study of Concentration Distributions in a Model Pore Electrode. I: Measurement of Two-Dimensional Concentration Gradients in a Zinc Model Pore," LBL-30133 (December 1990).
4. J. Weaver, F.R. McLarnon and E.J. Cairns, "Experimental and Theoretical Study of Concentration Distributions in a Model Pore Electrode. II: Mathematical Models and Comparison to Experiments," LBL-30134 (December 1990).

Surface Morphology of Metals in Electrodeposition

C.W. Tobias (Lawrence Berkeley Laboratory)

The objective of this project is to develop a pragmatic understanding of the processes and their interactions in the macrocrystallization of metals necessary for the design and optimization of rechargeable galvanic cells. Studies related to the surface morphology of metals include observation of thick deposits for groove patterns in flow cells. The deposit topography is measured by a Taylor-Hobson profilometer, while more-detailed images of surface structure are obtained by SEM and transmission electron microscopy (TEM). Electrolyte properties, including transport coefficients, are obtained by classical methods. Observations on nucleation frequency as a function of electrode overpotential are performed using steady-state and transient techniques. A special flow cell, equipped with the capability to take time-lapse photographs and real-time video recordings, is used to observe and record macroscopic crystal growth and the development of characteristic patterns in the electrodeposition of Zn. Microprofiled Pt electrodes, on which predetermined surface roughness elements are grafted by very large-scale integration (VLSI) process technology, serve as reproducible substrates for the study of propagation of patterns in macro-morphology. The growth of surface profiles is modeled by finite difference-finite element and boundary-element techniques for solution of the Laplace equation.

Zinc deposition from alkaline zincate electrolyte results, over a wide range of current densities and flow rates, in the development of porous, "mossy" Zn morphology. Videomicroscopic recording of the deposition process in a flow channel has revealed that moss formation is initiated only after a more or less substantial "compact" layer is deposited, when large

protrusions appear on the surface. Following the emergence of mossy structures on the surface, they propagate laterally as well as grow in thickness (Figure 7). The growth of the compact layer is stunted, if not stopped. The process is irreversible. At a constant fraction of the limiting current the compact layer thickness grows with increasing applied current density. Preliminary modeling efforts have shown that in the less-accessible areas of the surface (*i.e.*, between roughness elements) the hydroxyl-ion concentration is higher than in the bulk electrolyte, causing a shift in local electrode potential and an abrupt change in crystalline habit. The x-ray studies indicate a shift in the crystalline plane favored for growth relative to the deposition of Zn in the compact form.

The following studies of Zn deposition on well-defined micromosaic electrodes in acid halide electrolytes and Ni electrodeposition in the presence of inhibitors are beneficial for understanding the growth of different morphological structures, such as mossy Zn and dendrites that can form in alkaline Zn cells.

The influence of hydrodynamic flow and current density was investigated for Zn electrodeposition from acid chloride or bromide electrolyte. The num-

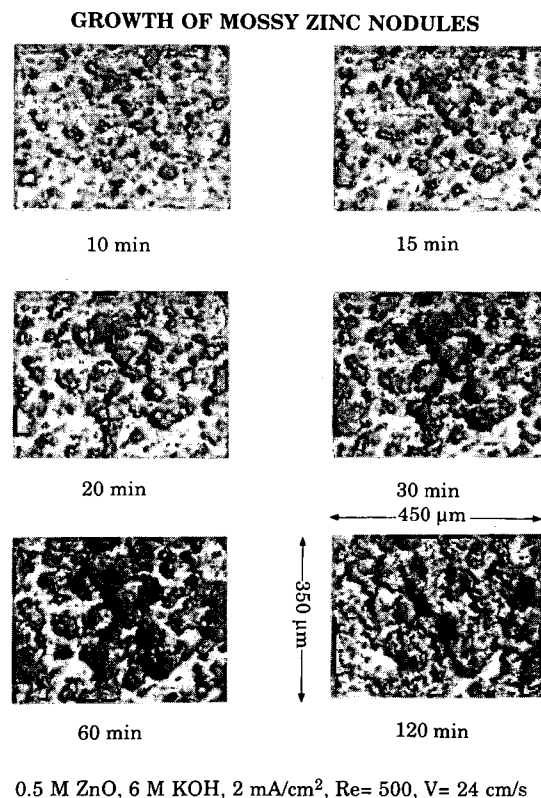


Figure 7. Growth of mossy Zn nodules.
(XBB-914-3287A)

ber density of striations that form is a strong function of current density, and they form over the entire electrode surface. The characteristic frequency of the striae was determined by spectral power estimation using fast Fourier transforms combined with profilometry (Figure 8). At lower current densities the striae are wider and have longer wavelengths. The power spectrum shows a quasi-gaussian distribution, consistent with sinusoidal waves with superimposed random, smaller scale roughness. Above a critical current density, the striae becomes too narrow to be morphologically stable and instead, meld. Thus at high current densities, Zn deposits are free of striations and are relatively less rough. The use of micron-scale patterned substrates yielded striated deposits under conditions where they would not normally form. This reinforces the hypothesis that striations result from interactions between emerging growth centers and the electrolyte flow.

To clarify the role of nodules in determining local mass-transport rates, the latest generation of stable micromosaic electrodes was employed. The new design, which was fabricated in the U.C. Berkeley microfabrication facility, has shown much-improved life over that of the earlier version because of the added Si_3N_4 passivation layer and the replacement of Cr with Ti. The nitride layer is deposited in a plasma-enhanced chemical vapor deposition (PECVD) reactor in three separate layers to avoid pinholes that would provide access to the underlying Al lines. Reactive-

ion etching of the nitride to form contacts to the mosaic elements was performed in a SiF_6 plasma. While this plasma is not selective between Si and Si_3N_4 , Al is an effective etch stop. The sputtered Ti layer insures adequate adhesion of the overlying Pt. Work completed to date includes design and fabrication of a flow cell which accommodate the micromosaic electrode along one side of the flow channel. The cell includes a micro-manipulator stage, which facilitates the precise placement of a wire obstacle perpendicular to one of the mosaic segments. The reduction of ferri- to ferro-cyanide will serve as the electrode reaction by which the mass-transfer boundary layer will be mapped out around the wire obstacle.

Leveling or smoothing of a microprofile in electrodeposition was studied both experimentally (Ni deposition) and theoretically (finite-element technique). The theoretical study was undertaken to clarify the role of recirculating flows in small cavities, of various shapes, in the electrode surface. The effect of Couette and Poiseuille flows passing by two-dimensional microscopic cavities was calculated by finite-element technique. Recirculation regions were characterized as a function of Reynolds number, notch shape and depth. The increase in transport rates caused by convective eddies was assessed relative to the pure diffusion case for various boundary-layer thicknesses. Secondary flows were shown to noticeably enhance transport of inhibitors into microscopic trenches only at high Peclet numbers (*i.e.*, at very high flow velocities).

The electrodeposition of Ni into an angular trench in the presence of coumarin, a widely used inhibitor, was simulated using various boundary-layer approximations that are representative of flow parallel or transverse to the groove. Based on the diffusion-adsorption mechanism of leveling action, the dependences of developing contours on the Langmuir coefficient and on the metal-ion/inhibitor flux ratio were investigated. Leveling efficiency was shown to be highest for thin, planar boundary layers, and lowest for contour-following boundary layers which result in simple geometric leveling. The model successfully predicts the leveling-off of the inhibitor effect with an increase in the ratio of inhibitor concentration to metal-ion flux, and that there is an optimal thickness for the mass-transfer boundary layer or flux of additive, which results in superior leveling performance. Satisfactory agreement was found between the predicted contours and experimental leveling efficiencies determined by previous investigators.

The effect of corrosive agents (for example Br_2) that are consumed at the transport-limited rate on developing metal deposit profiles has been character-

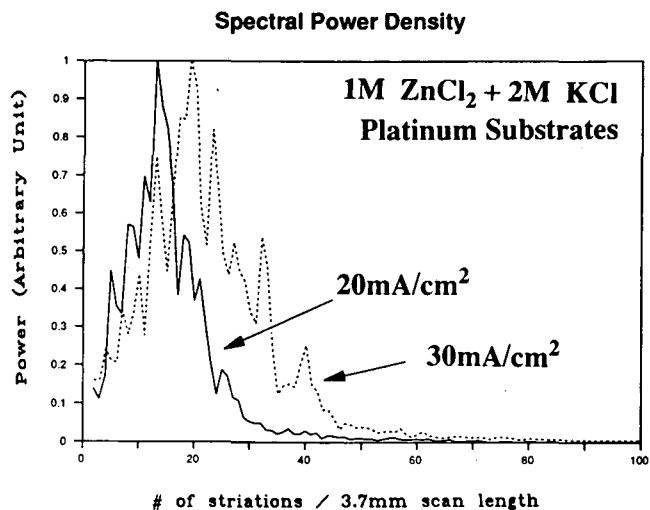


Figure 8. Spectral power density of striations in Zn deposits grown galvanostatically at 20 and 30 mA/cm^2 . The frequency of striations increases linearly with current density. These results are based on Fourier transforms of 27 separate profiles.

(XBL-9011-3548)

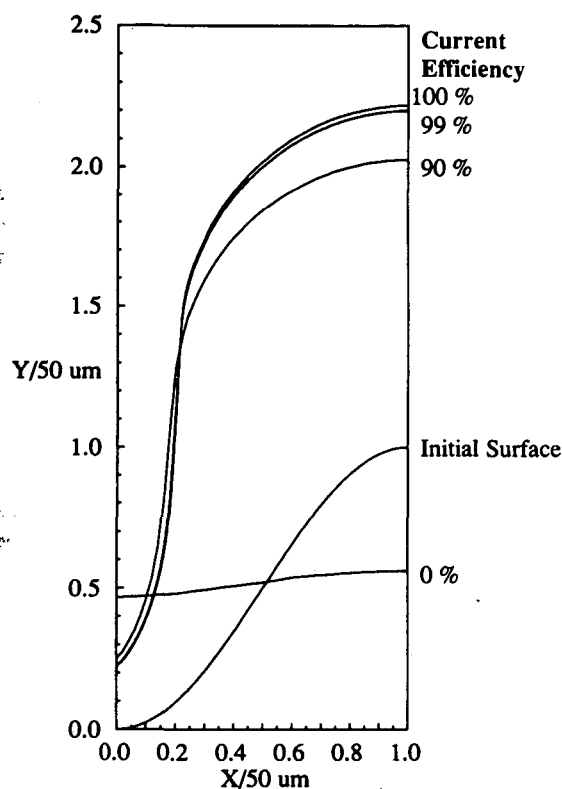


Figure 9. Surface contours in the simulated deposition of Zn from a bromide solution, at various levels of simultaneous corrosive attack by Br_2 . (XBL-9012-3954)

ized as a function of *i*) the relative rates of corrosion and electrodeposition, *ii*) the relative importance of ohmic and kinetic resistance in determining the current distribution, and *iii*) the geometry of the system. Corrosive agents are shown to blunt sharp features even for current efficiencies as high as 99% (Figure 9). Significant leveling occurs if the current distribution is dominated by charge-transfer kinetics and the rate of corrosion is on the order of the rate of electrodeposition.

PUBLICATIONS

1. K.G. Jordan, "Levelling of Microprofiles in Electrodeposition," *Ph.D. Thesis*, LBL-29924 (1990).
2. C.W. Tobias and K.G. Jordan, "The Effect of Inhibitor Transport on Leveling in Electrodeposition," LBL-29343 (1990).
3. C.W. Tobias and K.G. Jordan, "The Influence of Corrosive Agents in Electrodeposition on Microprofiles," LBL-30053 (1990).

B. LEAD/ACID CELLS

Lead/acid cells use positive electrodes of lead oxides which exist in different phase compositions and stoichiometry. The positive active material, formed electrochemically, is a major factor influencing the performance and life of the lead/acid battery. Thus, understanding the properties of these lead oxides would be helpful in promoting longer cycle life.

Battery Materials: Structure and Characterization

J. McBreen (Brookhaven National Laboratory)

The objectives of this project are to elucidate the molecular aspects of materials and electrode processes in batteries and to use this information to develop electrode and electrolyte structures with good performance and long life. Work during the year included EXAFS studies of materials related to the positive electrode in lead/acid batteries.

EXAFS and XANES Studies of Lead Oxides. In the initial part of the program x-ray absorption spectra (XAS) were obtained on lead oxides of known phase composition and stoichiometry. These oxides were prepared by methods described in the literature and all were characterized by x-ray diffraction. The oxides included red PbO , well-crystallized Pb_3O_4 , and several preparations of $\alpha\text{-PbO}_2$ and $\gamma\text{-PbO}_2$. XAS at the Pb L_{III} edge were obtained for these prepared samples and also for Pb foil, yellow PbO , 0.5 M aqueous $\text{Pb}(\text{ClO}_4)_2$ and 0.06 M $\text{Pb}(\text{C}_2\text{H}_3\text{O}_2)_4$ in glacial acetic acid. Analysis by EXAFS of the two solutions showed that the Pb^{2+} ions were coordinated with 12 waters of hydration with a Pb-O distance of 0.248 nm, and the Pb^{4+} ions were coordinated with 6 acetate groups in a unidentate configuration with a Pb-O distance of 0.223 nm. The XANES features were consistent with an icosahedral coordination of Pb^{2+} ions and an octahedral coordination of Pb^{4+} ions. A comparison of the XANES for Pb, 0.5 M $\text{Pb}(\text{ClO}_4)_2$ and 0.06 M $\text{Pb}(\text{C}_2\text{H}_3\text{O}_2)_4$ shows the expected shifts in edge energy with oxidation state. In the case of $\text{Pb}(\text{C}_2\text{H}_3\text{O}_2)_4$ there was a well-defined pre-edge absorption due to the $2p \rightarrow 6s$ transition. There are marked differences in the EXAFS for $\alpha\text{-PbO}_2$ and $\gamma\text{-PbO}_2$. In the case of $\gamma\text{-PbO}_2$ there are peaks in the radial structure function out to 0.8 nm. This is due to focusing effects from the aligned Pb atoms in the rutile structure. No such alignment occurs in the orthorhombic structure of $\alpha\text{-PbO}_2$ and there are no peaks beyond 0.4 nm. The XANES features for the

oxides could be explained on the basis of hybridization, site symmetry and crystal field splitting effects. The increased distortion in octahedral coordination on going from $\text{Pb}(\text{C}_2\text{H}_3\text{O}_2)_4$ to $\gamma\text{-PbO}_2$ to $\alpha\text{-PbO}_2$ decreases the intensity of the white line in the XANES spectra. The intensity of the pre-edge absorption for PbO_2 depends on the method of preparation and has been correlated with the oxide stoichiometry. The XANES for yellow PbO are consistent with a C_{2v} symmetry and equal bond lengths for both the long and short Pb-O bonds.

EXAFS Studies of Battery Electrode Materials. Formed battery plates supplied by Johnson Controls, Inc. were investigated. XANES results indicated that the stoichiometry of the $\gamma\text{-PbO}_2$ in the formed plates was lower than that found for electrochemically or chemically prepared $\gamma\text{-PbO}_2$. Chemically prepared PbO_2 is inactive as a battery material. XANES results also show that the stoichiometry of electrochemically prepared PbO_2 is lower when it is deposited from solutions containing antimony. This strongly indicates that electrochemical activity is related to stoichiometry and that the beneficial effect of antimony is related to effects on PbO_2 stoichiometry.

PUBLICATIONS

1. K.I. Pandya, W.E. O'Grady, D.A. Corrigan, J. McBreen and R.W. Hoffman, "Extended X-ray Absorption Fine Structure Investigations of Nickel Hydroxides," *J. Phys. Chem.*, **94**, 21 (1990).
2. K.I. Pandya, R.W. Hoffman, J. McBreen and W.E. O'Grady, "In-Situ X-ray Absorption Spectroscopic Studies of Nickel Oxide Electrodes," *J. Electrochem. Soc.*, **137**, 383 (1990).
3. J. McBreen, "The Nickel Oxide Electrode," in *Modern Aspects of Electrochemistry*, Vol. 21, J.O'M. Bockris, B.E. Conway, and R.E. White, Eds., Plenum Press, New York (1990) p. 29.
4. J. McBreen, "EXAFS and XANES Studies of Lead Oxides and Solutions of Pb(II) and Pb(IV) Ions," BNL-45832 (1990).
5. D. Guay, G. Tourillon, E. Dartyge, A. Fontaine, J. McBreen, K.I. Pandya and W.E. O'Grady, "In Situ Time-Resolved EXAFS Study of the Structural Modifications Occurring in Nickel Oxide Electrodes Between Their Fully Oxidized and Reduced State," BNL-45803 (1990).

C. COMPONENTS FOR HIGH-TEMPERATURE CELLS

Superior alternatives to the $\beta''\text{-Al}_2\text{O}_3$ ceramic electrolyte and high-temperature sulfur-polysulfide electrode for Na/S cells, and stable components for Li/S cells are under investigation.

High-Temperature Cell Research

E.J. Cairns and F.R. McLarnon (Lawrence Berkeley Laboratory)

The objectives of this research are to investigate new electrodes, electrolytes and other cell components, and to determine the fundamental mechanisms of capacity loss of the electrodes, as well as means for eliminating the losses. Experimental studies of candidate materials for high-temperature cells are augmented by mathematical modeling of electrode behavior during cycling.

Mathematical Modeling. A comprehensive model of the sulfur electrode in Na/S cells has been developed. The cell being modeled is of the tubular central-sodium type, and includes a thin layer of $\alpha\text{-Al}_2\text{O}_3$ felt around the $\beta''\text{-Al}_2\text{O}_3$ solid electrolyte to prevent deposition of sulfur on the solid electrolyte during cell charge. The model consists of a set of nonlinear partial differential equations (PDEs) which describes the processes of diffusion, migration, and convection that take place during the operation of such a cell. Linearization of these highly nonlinear equations and their boundary conditions has been accomplished by implementation of a symbolic equation manipulator, written in "Mathematica." The Mathematica program automatically generates the corresponding banded matrices used in the Newman-IAD (implicit alternating direction) technique for solving time-dependent PDEs. This work results in a tremendous reduction of the tedious effort necessary to linearize the PDEs and to generate the corresponding matrices necessary for numerical solution. Solution of the linearized equations is presently being performed on the UC Berkeley Cray X/MP computer *via* implementation of the Newman-IAD method, which is a numerical technique for solving the finite-difference equations which arise in the solution of second-order linear PDEs.

Phosphorus/Sulfur Electrode Studies. The addition of phosphorus to the sulfur cathode in the Na/S cell may improve power output by reducing Na⁺-ion transport resistance. This may be accomplished by decreasing the viscosity of the cathode melt, thereby allowing faster transport of Na⁺ ions in the melt, decreasing cell overpotential and increasing its power output. Efforts continue to develop an experimental cell that will permit the evaluation of optimal P/S ratios *via* equilibrium EMF measurements at temperatures up to 500°C. The cell uses solid ceramic β''-Al₂O₃ electrolyte, and is constructed much like standard Na/S cells. Most of the effort has been directed at improving the cell design so that a demountable hermetic seal is maintained at elevated temperatures.

Sodium/Metal Chloride Cell Research

D.R. Vissers (Argonne National Laboratory)

The objective of this research program is to generate the technical base of information needed to develop advanced sodium/metal chloride (Na/MCl₂) cells with high specific energy (200 Wh/kg at the 3-h rate) and power (>200 W/kg at 80% DOD). The present cell uses a molten Na negative electrode, a β''-Al₂O₃ solid electrolyte, and a solid metal chloride such as NiCl₂ or FeCl₂ for the positive electrode. The metal chloride cathode uses a secondary electrolyte (catholyte) of NaAlCl₄. The cell is normally operated at 260°C. Despite the high theoretical specific energy of the Na/NiCl₂ cell (790 Wh/kg), the performance of the present β''-Al₂O₃ single-tube cells is limited (~100 Wh/kg and ~100 W/kg). Our preliminary cell modeling studies suggest that, to develop high-performance Na/MCl₂ cells, it will be necessary to increase the area of the solid β''-Al₂O₃ electrolyte and to operate at low-to-moderate current densities.

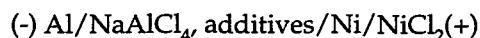
Our cathode development studies have focused on increasing the performance of the NiCl₂ electrode. In these studies, annular NiCl₂ electrodes were operated inside a β''-Al₂O₃-tube electrolyte. These electrodes contained between 15 and 20 vol% Ni and possessed a high capacity density, 0.40-0.50 Ah/cm³. These capacity densities are almost 50% greater than those used in the state-of-the-art cells. Last year we found that an 18 vol% Ni electrode had an ASI of 1.2 ohm-cm² at 300°C. By fabricating the electrodes with higher and more uniform porosity, we obtained a significant decrease in the ASI. A 20 vol% Ni electrode (4-mm diameter, 1-cm tall) made by a new fabrication method had an ASI of 0.80 ohm-cm² at 260°C. At lower Ni fractions, similar improvements in ASI were

observed. In an electrode containing 17 vol% Ni, for example, ASIs as low as 0.5 ohm-cm² were obtained at 260°C. Clearly, these values are lower than those of the state-of-the-art cells (1.0-1.5 ohm-cm²); the fabrication method plays an important role in determining the ASI.

Additional improvements in the performance of these and larger porous electrodes will be realized through changing the morphology and chemistry of the electrode. For this purpose, we are investigating the effects of fabrication parameters on electrode morphology and elucidating the kinetics and mechanisms of the electrochemical processes. Several structural aspects of the Ni electrode, observable under the microscope, may limit its performance. Among them are nonuniform distributions of Ni and NaCl. Microscopic examination of post-test NiCl₂ electrodes revealed an obvious segregation of material, with the NaCl particles clustering together and, in some places, forming strata. This segregation would leave other areas of the electrode deficient in NaCl. If the distribution of NaCl were more uniform, the resulting NiCl₂ layer would also be more uniform. As a consequence, the ASI at deep discharge would be lower. Work is underway to improve the distribution of electrolyte and active material within the electrode and the resulting morphology.

Altering the chemistry of the electrode should also help improve electrode performance. As such, further NiCl₂ electrode development will require a thorough understanding of the kinetics and the mechanisms of the electrode processes occurring during cell operation. Three techniques are being used in these investigations: *i*) interrupted galvanostatic cycling of nonporous electrodes, *ii*) cyclic voltammetry of nonporous electrodes, and *iii*) interrupted galvanostatic cycling of Na/β''-Al₂O₃/NiCl₂ cells built with porous positive electrodes.

The first two techniques were developed to better understand the electrode processes occurring on a simple nonporous Ni electrode surface (0.15-cm-diameter Ni wire) in various NaCl-saturated chloroaluminate electrolytes. Here, the processes occurring on the surface may be clearly observed without the complications due to a porous structure. The cell used in these studies can be depicted schematically by:



Use of an Al counter electrode has the following advantages: *i*) acts as both a counter and reference electrode because of its well-defined chemistry and fast kinetics, *ii*) yields results that can indicate the type of

soluble Ni species present, and *iii*) makes cell construction simple. Galvanostatic cycling and cyclic voltammetry with a nonporous electrode are used in a complementary fashion to gain insight into the fine details of electrode kinetics.

The third technique studies the performance of the porous electrode in the complete Na/NiCl₂ cell. The complete cell is designed in such a way that the properties of the three main cell components (Na electrode, β"-Al₂O₃ solid electrolyte, and NiCl₂ electrode) can be evaluated to find limiting factors that influence the overall cell performance. The cell containing the porous electrode is operated under a one-dimensional current distribution. From the results of the tests, the important cell parameter, ASI for a 15-s potential relaxation (ASI_{15s}), can be determined as a function of temperature, cycling regime, and cycle life. These values are indicative of the intrinsic properties of the electrode and, therefore, can be used in modeling calculations and cell scaleup.

The most significant information gained from these investigations is summarized below. During charge NiCl₂ forms a poorly conducting layer on the surface of the Ni electrode, which produces a marked increase in the ASI_{15s} of the electrode (compare curve at 20% active-material utilization with that at 90% in Figure 10). Upon reaching a certain thickness, this layer hinders further charge of the electrode. This situation is characterized by a limiting area capacity (units of C/cm²), which is a strong function of temperature (Figure 10). Cyclic voltammograms and charge-discharge curves of nonporous electrodes indicated that the charge process takes place in two consecutive steps. The reactions associated with these steps are not understood and are being investigated further.

Additives greatly influence the electrode charge-discharge process and, consequently, the limiting area capacity and ASI. We found that 2 wt% sulfur additive in nonporous Ni electrodes increases the limiting area capacity by a factor of about five, decreases the ASI_{15s} by a factor of about two, and improves the coulombic efficiency by up to 100%. The observed improvement in coulombic efficiency of the cell suggests that an insoluble, sulfide-containing Ni species forms on the Ni electrode surface. This NiCl₂ + S mixture has substantially better performance characteristics than NiCl₂ alone.

As an aid for the further development of the Ni electrode, we have mathematically modeled its electrochemical behavior. The most important factor in Na/MCl₂ cell modeling is determining the impedance of the positive electrode during discharge. Sodium/metal chloride cells have higher impedance than

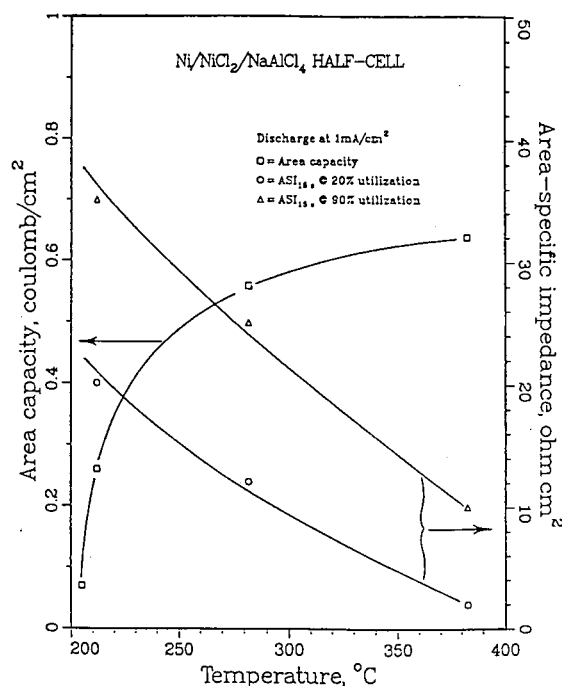


Figure 10. Performance characteristics of nonporous NiCl₂ electrode discharged at 1 mA/cm² as function of temperature. (XBL 917-1425)

Na/S cells of the same configuration, primarily due to the added resistance associated with the catholyte in the pores of the cathode. The NaAlCl₄ is only a moderately good ionic conductor. The transport of Na ions through the liquid electrolyte accounts for a large portion of the total electrode impedance, as reported in the literature for cells having thick electrodes (~1 cm). The reaction impedance is an important factor if the electrode is thin, the temperature is well below 250°C, or the discharge is nearing completion. All of these conditions are of interest in designing Na/MCl₂ cells for the optimum combination of high specific energy, high specific power, and operability over a wide temperature range.

We developed a finite-element model for cells having cathodes inside β"-Al₂O₃ electrolyte tubes. In this model, the electrode is divided into tubular elements of equal volume. The metal matrix has negligible resistance and the reaction impedance within an electrode element is inversely proportional to the unreacted NiCl₂ capacity in that element. The calculation of the electrode impedance is an iterative process for each one percent of the capacity discharged. Calculations made for 10 and 20 volume elements resulted in the same electrode impedance within 0.5% over the discharge range 0.5 to 94.5%.

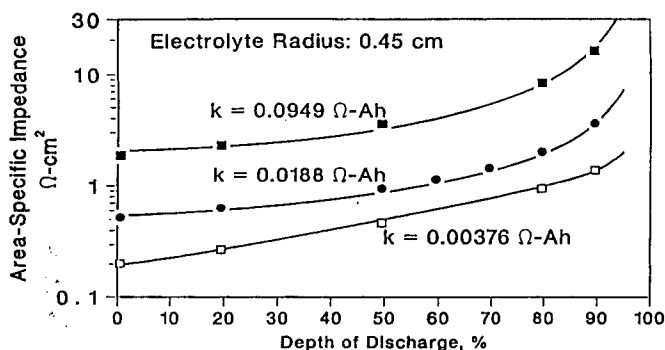


Figure 11. ASI calculated from empirical equation (solid lines) and finite element model (points).
(XBL 917-1426)

Calculations were made for the conditions used in obtaining experimental data from testing a Na/NiCl₂ cell with a capacity density of 0.354 A/cm³, an electrode radius of 0.45 cm, and a current collector radius of 0.24 cm. In these calculations, the value of the reaction impedance is constant, which we refer to as the "capacity specific resistance" (in units of W-Ah), and was varied until the calculated impedances were in close agreement with the measured values over the discharge range (Figure 11). This indicates that our finite-element model accurately reproduces the true impedance conditions over the course of the discharge.

PUBLICATIONS

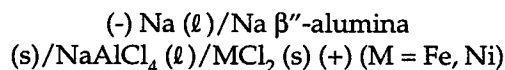
1. S.L. Marshall and L. Redey, "Mathematical Analysis of a Four-Point Conductivity Probe for Cylindrical Samples," *Review of Scientific Instruments*, **61**, 2659 (1990).
2. I. Bloom, P.A. Nelson, L. Redey, S.K. Orth, C.L. Hammer, R.S. Skocypec, D. Dees, M.C. Hash, and D.R. Vissers, "Design Considerations for the Development of Advanced Sodium/Metal-Chloride Cells," *Proc. of the 25th Intersoc. Energy Conversion Eng. Conf.*, Reno, NV, August 12-17, 1990, Vol. 3, p. 341.
3. D.R. Vissers, I.D. Bloom, M.C. Hash, L. Redey, C.L. Hammer, D.W. Dees, and P.A. Nelson, "Development of High-Performance Sodium/Metal-Chloride Cells," *DOE/EPRI Beta Battery Workshop*, Chester, England, June 12-14, 1990.

New Battery Materials

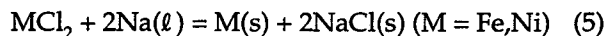
R.A. Huggins (Stanford University)

The objective of this program is to develop and characterize materials which have potential applications in high-performance secondary battery systems. The emphasis is to understand the relationships between fundamental thermodynamic and kinetic parameters (e.g., phase equilibria, Gibbs' free energy values and chemical diffusion within solid phases, and the microscopic and macroscopic electrochemical phenomena) that influence the behavior of battery materials.

During 1990, the efforts have been directed toward studies of the Na-metal chloride system, with particular attention to the kinetics of the positive electrode. This battery system operates at approximately 250°C, which is somewhat lower than that necessary for the Na/S system, and employs the following liquid/solid/liquid/solid (L/S/L/S) configuration:



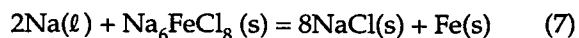
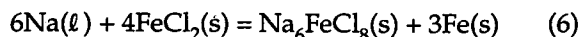
The cell reaction may be written in a simplified form as:



leading to open-circuit cell voltages of 2.35 and 2.59 V for FeCl₂ and NiCl₂, respectively, at an operating temperature of 250°C. In the case M = Fe, the name "Zebra cell" has been employed, while the name "Cheeta cell" has been applied in the case of M = Ni.

Simplified isothermal phase diagrams at 250°C have been calculated for the Na-Fe-Cl and Na-Ni-Cl systems. These diagrams predict that the observed cell reactions will occur at cell voltages of 2.34 and 2.60 V for M = Fe and Ni, respectively, in excellent agreement with the experimentally observed values mentioned above.

For the case M = Fe, structural work has shown that an intermediate phase in the FeCl₂-NaCl system, Na₆FeCl₈, is formed during discharge at 250°C *via* the solid-state displacement of metallic Fe, leading to the following cell reactions:



The formation of this intermediate phase does not significantly affect the dynamic cell discharge voltage or kinetic behavior; however, the free energy of formation of Na_6FeCl_8 from NaCl and FeCl_2 , calculated from the coulometric titration data, is very low.

The formation of an intermediate phase apparently does not occur when $M = \text{Ni}$. At higher temperatures, two additional ternary phases, Na_2FeCl_4 and $\text{Na}_2\text{Fe}_3\text{Cl}_8$, are formed. The formation of eutectic compositions in the Na/FeCl_2 and Na/NiCl_2 systems at 370 and 570°C respectively, limit the maximum operating temperatures of the Zebra and Cheetah cells to ~300 and 500°C, respectively.

In the case $M = \text{Fe}$, at positive electrode potentials above 3.65 V vs Na, FeCl_2 becomes oxidized to FeCl_3 . This latter phase is soluble in the molten salt electrolyte, leading to poisoning of the ceramic solid electrolyte separator. In order to avoid this and provide overcharge protection, Ni metal is added to the positive electrode matrix which is oxidized to NiCl_2 before (i.e., at a lower potential vs Na) FeCl_2 is oxidized to FeCl_3 . It is also important to maintain the composition of the NaAlCl_4 electrolyte on the NaCl side of the exact stoichiometry.

PUBLICATIONS

1. B.T. Ahn and R.A. Huggins, "Preparation, Structures and Conductivities of Li_2SiS_3 Phases," *Materials Res. Bull.*, **25**, 381 (1990).
2. S. Crouch-Baker, G. Deublein, H-C. Tsai, L.Z. Zhou and R.A. Huggins, "Materials Considerations Related to Sodium-Based Rechargeable Cells for Use Above Room Temperature," *Solid State Ionics*, **42**, 109 (1990).

D. CORROSION PROCESSES IN HIGH-SPECIFIC-ENERGY CELLS

These projects aim to develop low-cost containers and current-collector materials for use in nonaqueous, alkali-sulfur, and other molten-salt cells.

Corrosion-Resistant Coatings for High-Temperature High-Sulfur-Activity Applications

J.R. Selman (Illinois Institute of Technology)

The objective of this research is to develop corrosion-resistant coatings for cell components that are exposed to high-sulfur-activity environments in Li/FeS_2

and Na/S batteries. This research is directed at developing technology for the production of molybdenum-based and titanium-based coatings by electrochemical or chemical vapor deposition (CVD) processes.

Optimized Deposition of Molybdenum and Molybdenum Carbide. A scale-up effort was undertaken to plate Mo_2C layers on much larger samples using the experience based on the MSECD (Molten Salt Electrochemical Deposition) experiments. The cell which had initially been used to coat small flag coupons was modified to accommodate the substantially larger canisters for Na/S batteries. Cylindrical low-carbon steel canisters supplied by Chloride Silent Power Ltd. (CSPL, Runcorn, UK) were internally coated with Mo_2C for tests in an actual Na/S battery environment. These containers have a total volume of 65 cm³ and an internal surface area of 75 cm². Similarly, a number of cylindrical current collector rods supplied by ANL were coated.

Preliminary studies of the corrosion behavior of the coating developed under this program were initiated at CSPL, and a number of coated current collectors were returned to ANL for evaluation.

Reports were received from CSPL and ANL for in-cell testing of Mo_2C -coated Na/S battery cans and out-of-cell testing of Mo_2C -coated current collectors for Li-alloy/ FeS_2 cells, respectively. In general, the results were encouraging though further optimization of coating quality is necessary.

A new series of experiments was started to verify the feasibility of obtaining Mo_2C coatings from non-fluoride, oxide-based melt. A molten bath consisting of an equimolar mixture of Na_2WO_4 and K_2WO_4 was used in these experiments. The Mo and carbon species are introduced as alkali molybdate and alkali carbonate by direct mixing with the base tungstates as a powder. The electrolyte composition is being varied to determine the influence of type and amount of alkali molybdate and carbonate on the deposit.

One of the main advantages of MSECD from oxide-based melts is that the melt does not require handling in an inert atmosphere. All experiments were carried out under ambient atmosphere without further precautions. The procedure that was adopted in the plating process was as follows, in most cases: *i*) an initial cathodic pulse to achieve high nucleation density, *ii*) current reversal, and *iii*) a decreasing cathodic current. Microscopic examination of the coating at the sample surface is carried out to assess the morphology, continuity and density of the coating. Results to date indicate that a carbide coating of good quality can be obtained, according to optical characterization and metallographic analysis of the most successful cases. However, the coating morphology

depends strongly on the temperature and melt composition. Higher temperature tends to produce larger grains. Relatively good-quality coatings were obtained in Li-containing melts with a typical current density of up to 50 mA/cm².

Preparation of Mo and Mo₂C by PECVD. The PECVD equipment was assembled and a glow discharge plasma generated using Ar. The steady-state plasma was generated in 1 to 2 min by a RF power source applied after a stationary flow at approximately 0.5 to 2 torr pressure was established. A system was installed to heat the substrate by ohmic resistance. In the above pressure range, a maximum sample temperature of about 350°C was obtained in 40 min. By keeping the pressure low and stationary, with Ar gas flowing evenly, and by supplying power gradually from an RF generator, one can generate a glow discharge in the steady state. Once the resistance-heated sample holder has reached a sufficient temperature, CVD starts. The solid molybdenum carbonyl, which serves as the precursor, is contained in the saturator reservoir and its sublimation pressure is controlled by regulating the reservoir temperature. Thus, the desired dilution of carbonyl in Ar gas, at 0.5 to 2 torr total pressure in the chamber, is achieved easily by heating the saturator slowly.

Initial experiments show that Mo or Mo₂C thin films may be obtained by PECVD with molybdenum carbonyl as the precursor. The thickness of the film produced by 40-min deposition was about 0.3 mm, as estimated from diffraction analysis. The presence of Mo and/or Mo₂C in the thin-film sample was detected by electron diffraction analysis. The x-ray spectra suggest that the structure of the Mo or Mo₂C film is amorphous.

Corrosion, Passivity, and Breakdown of Alloys Used in High-Energy Batteries

J. Kruger and P. Moran (The Johns Hopkins University)

The overall objective of this project is to investigate the phenomena of passivation and its breakdown on metals and alloys in nonaqueous solvents for rechargeable Li batteries. Since passive layers influence and control corrosion rates, understanding the corrosion phenomena is crucial to the selection and development of corrosion-resistant materials. In 1990, the work centered on completion of corrosion studies on 304 stainless steel in propylene carbonate (PC) with 0.5 M LiAsF₆ and on preliminary studies of Armco iron and 1018 carbon steel in dimethoxyethane (DME)/0.5 M LiAsF₆.

Stainless steel 304SS with an air-formed film is passive in clean anhydrous PC/LiAsF₆ at potentials up to 4.2 V (relative to Li/Li⁺). Potentiodynamic scans of 304SS in PC/LiAsF₆ that contains common PC impurities (e.g., propylene oxide, propylene glycol, water) were performed to study their effects on passivation and the breakdown of passivity. The addition of 500-ppm water or propylene oxide to anhydrous PC/0.5M LiAsF₆ solutions raised the breakdown potential on 304SS to between 4.4 and 4.5 V. It is believed that these low levels of propylene oxide or water are sufficient to protect the 304SS by oxide formation or by aiding the formation of a more protective salt film when PC adsorption is no longer possible. The addition of propylene glycol (10,000 ppm) to PC/LiAsF₆ has little effect on the corrosion behavior of 304SS. The addition of as little as 5 vol% PC/LiClO₄ to PC/LiAsF₆ solutions raises the breakdown potential of 304SS to 4.8 V, approximately equivalent to the breakdown potential on 304SS in pure anhydrous PC/LiClO₄ solutions. However, mechanical disruption by scratching the stainless steel surface in mixed PC/LiAsF₆-LiClO₄ solutions at potentials greater than 4.2 V and below the perchlorate oxidation potential causes rapid corrosion. The addition of small amounts PC/perchlorate is insufficient to adequately repassivate the defects that develop in the air-formed film.

The oxidation of DME in DME/LiAsF₆ electrolytes is an important factor in the passivation and corrosion behavior of alloys. The approximate oxidation potentials relative to the Li potential are: oxidation of DME = 4.25 V, and oxidation of AsF₆⁻ = 5.15 V. Another reaction occurs at about 4.55 V; this is presently unidentified.

Preliminary studies of Armco iron and 1018 carbon steel were conducted in DME/0.5 M LiAsF₆ solutions with a water content of about 300 ppm. The air-formed film on both the Fe and the carbon steel in these DME/LiAsF₆ solutions is stable at potentials less than 5.1 V. When this air-formed film is mechanically removed *in situ*, repassivation occurs quickly by adsorption of DME molecules or the precipitation of an iron hexafluoroarsenate salt film. The potentiodynamic scans of Fe and carbon steel show no active-passive transition, but have a good passive region up to the oxidation of the salt, beyond which active dissolution leads to massive pitting as evidenced by post-scan SEM analysis.

Potentiostatic holds of Armco iron or 1018 carbon steel during removal of the air-formed film by *in situ* scratching displayed rapid repassivation (2-7 sec) at potentials below 4.6 V. Between 4.6 and 4.8 V, the repassivation time and charge passed during

repassivation both increased with increasing potential. SEM showed no evidence of a salt film deposit in the scratches of either the Fe or carbon steel samples, and x-ray microanalysis (XRM) showed no evidence of As either inside or outside the scratches for holds below 4.8 V. This indicates that repassivation is not caused by precipitation of a $\text{Fe}(\text{AsF}_6)_2$ or $\text{Fe}(\text{AsF}_6)_3$ salt at these potentials. It is not yet clear whether the amount of charge passed during repassivation is consistent with a mechanism of solvent chemisorption. At 4.8 V for carbon steel and 4.9 V for Armco iron, the "hold-and-scratch" experiments led to a very sluggish repassivation of the respective scratches, on the order of an hour. SEM examination revealed the existence of a film within the scratches. XRM showed that As was present in the scratches and absent outside the scratches. This indicates that passivation at 4.8 V for the steel and 4.9 V for Fe is controlled by the formation of precipitated $\text{Fe}(\text{AsF}_6)_2$ or $\text{Fe}(\text{AsF}_6)_3$ salt film. The upper end of the salt-film stability range is defined by the oxidation potential of the AsF_6^- anion (about 5.15 V).

Future studies will be conducted to assess the domains where the various passivating mechanisms (air-formed film, solvent chemisorption, salt film or polymerization) occur on Fe and carbon steel in anhydrous DME/ LiAsF_6 solutions. Following this understanding of Fe and carbon steel in the anhydrous DME/ LiAsF_6 solutions, intentional additions of water will be examined. Similar studies of pure Ni and 304SS in DME/ LiAsF_6 will be conducted. This will eventually lead to studies of all four metals and alloys in PC/DME mixtures with LiAsF_6 as the supporting electrolyte.

E. COMPONENTS FOR AMBIENT-TEMPERATURE NONAQUEOUS CELLS

Metal/electrolyte combinations that improve the rechargeability of ambient-temperature nonaqueous cells are under investigation.

Spectroscopic Studies of the Passive Film on Alkali and Alkaline Earth Metals in Nonaqueous Solvents: A Surface Science Approach

D.A. Scherson (Case Western Reserve University)

The main objective of this research is to elucidate the structure of passive films that form on alkali and alkaline earth metals in nonaqueous solvents. Recent efforts in the area of Li-based rechargeable batteries

have been aimed at exploring alternative electrolytes which might improve the the charge-discharge performance characteristics, with much of the attention being focused on SPEs.

Attenuated Total Reflection Fourier Transform Infrared Spectroscopy (ATRFTIRS) was used for the *in situ* study of the vibrational properties of the lithium/poly(ethyleneoxide) (PEO) interface. In order to avoid interferences associated with adventitious films and other impurities present on the metal surface (prior to contact with the electrolyte), Li was electrodeposited onto a semi-transparent inert metal film which was sputtered on a Ge ATR element using a carefully designed, hermetically sealed, two-electrode spectroelectrochemical cell.

The PEO films were prepared by dissolving the polymer in a LiClO_4 /acetonitrile (AN) solution. A small aliquot of the PEO/ Li^+ solution was placed on a glass plate (in a glove-box) and subsequently extended using a film applicator. The films that formed were dried under highly controlled conditions to yield an approximate thickness of 0.05 to 0.6 mm. A gold film (about 5-nm thick), was first sputtered onto a Ge ATR element and then covered along a three-side perimeter by a much thicker (~100 nm) Au film. The electrochemical cell was assembled inside the glove-box by placing a PEO/ LiClO_4 film (7 mm \times 32 mm) in the center portion and a Kapton gasket (0.05-mm thick) along the perimeter of the Ge prism so as to leave a gap of about 1 mm between the two components. A Li strip was then placed on top of the PEO film/Kapton assembly using a sputtered Ni film on a glass slide as a current collector. The cell was clamped together using a mechanical clip and a small amount of Amojoil (Aldrich Chemical Co.) which was applied to the side of the Kapton gasket to prevent air and moisture from entering into the main cell compartment. Electrochemical measurements were performed in the potentiostatic mode by using the Li foil as a reference/counter electrode. The data are presented in the form of $\Delta R/R = (R_{\text{sample}} - R_{\text{ref}})/R_{\text{ref}}$ where R represents the spectra obtained at the potential of interest and R_{ref} that obtained at a reference value. In this case R_{ref} corresponds to the spectra of the interface at the initial open circuit potential (1.57 V vs Li/Li⁺) for which the Au/PEO interface may be regarded as intact.

Figure 12 shows a series of *in situ* potential-difference ATRFTIRAS spectra obtained for the PEO/ LiClO_4 interface polarized at the specified values in the indicated sequence using the spectra collected at open circuit as a reference. As shown in the figure, no changes could be observed for the electrode polarized at +0.5 V vs Li/Li⁺(PEO). This is not surprising as no

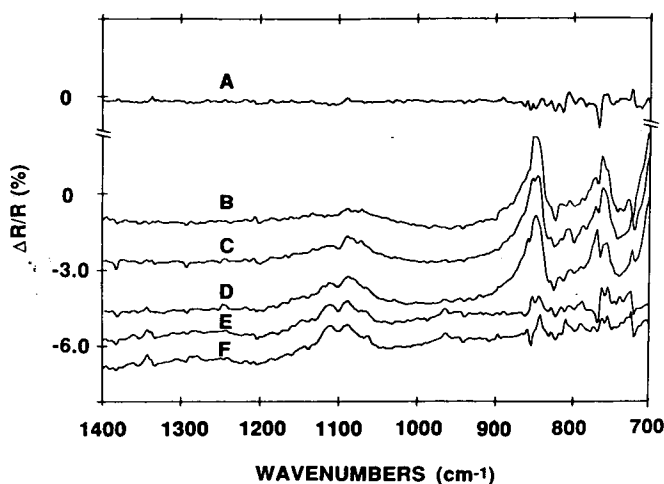
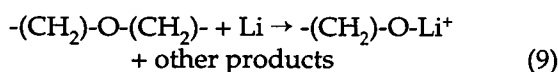


Figure 12. *In situ* potential-difference ATRFTIRAS spectra of a Au/Ge/PEO(LiClO₄) interface, using as a reference the spectra recorded prior to Li electrodeposition (bare Au/Ge/PEO(LiClO₄)). The spectra were acquired in the order A: 0.5; B: 0.0; C: -0.50; D: -0.75; E: -1.0; and F: -1.2 V vs Li/Li⁺ in PEO. (XBL 917-1427)

Li bulk deposition would be expected at this potential. The pronounced features in the region between 750 and 900 cm⁻¹ could be clearly observed when the Au/Ge electrode was polarized at 0.0 V. These changes, however, are most likely associated with modifications in the intrinsic properties of the Ge semiconductor substrate induced by a shift in the position of the Fermi level. In addition to these substrate-related bands, at least three other features could be observed in the region between 1000 and 1300 cm⁻¹. The positive-going band at ~1090 cm⁻¹ may be ascribed to the depletion of perchlorate ions in the neighborhood of the Au/Ge(PEO) interface. This observation, in addition to the decrease in the background reflectivity, is consistent with the deposition of Li on the Au/Ge surface, a process that would induce perchlorate migration toward the bulk electrolyte in order to satisfy electroneutrality. Most interesting, however, are the appearances of a well-defined peak at 1110 cm⁻¹, a wavelength associated with ether-type bonds, and the rather broad, ill-defined peak at 1200 cm⁻¹. These features are consistent with the cleavage of ether-type bonds and the formation of alkoxide functionalities, respectively, *i.e.*,



A similar reaction pathway has been proposed for the reaction of Li with tetrahydrofuran (an aliphatic cyclic ether) using FTIR in the (external) reflection absorption mode. As the potential was stepped in the positive direction, the band at 1090 cm⁻¹ was found to decrease and finally become negative going at a potential of 1.5 V. This can be attributed to the stripping of the deposited Li which would induce a replenishment in the amount of perchlorate in the region near the Au/Ge electrode to maintain charge neutrality.

***In Situ* Raman Spectroscopy of Lithium Electrode Surfaces in Alkaline Cells**

H. Tachikawa (Jackson State University)

The objective of this project is to characterize the surface layers on Li electrodes in nonaqueous electrolytes by *in situ* Raman spectroscopy. The formation of a passive layer on cathodically deposited Li has a strong influence on the rechargeability of secondary Li batteries. Characterizing the nature of the passive layer on Li electrode surfaces should provide information which is useful for improving the cycle life of secondary Li batteries. A thin-layer cell, which has a very narrow gap (~1 mm) between the working electrode and a quartz window, and a conventional two-compartment cell were used to record *in situ* Raman spectra of passive layers on a Li electrode surface. Lithium ribbons were used as the reference electrode and the counter electrode. Thin films (50-200 Å) of Li were cathodically deposited on either a smooth thin-film Ag surface or an anodized thin-film Ag electrode. Several combinations of solvents (including mixed solvents) and supporting electrolytes were used for Raman spectroscopic studies of the Li surface to investigate the reactivity of Li with the solvent and also to identify the passive films which form.

Dimethyl carbonate (DMC) and diethyl carbonate (DEC) were used as solvents. They were used singly, or mixed with either methyl acetate (MA) or methyl formate (MF). Either 1 M LiAsF₆ or 1 M LiClO₄ was used as the supporting electrolyte. At the smooth Ag electrode, strong Raman scatterings from the solvent, supporting electrolyte, and an unknown species (possibly from passive layers) were observed after depositing a thin Li film (50 Å). The intensities of the Raman bands decreased when thicker Li films (>500 Å) were deposited. The observed high-intensity Raman bands originated from surface-enhanced Raman scatterings, which may have been created by the small particles of Li on the smooth Ag surface. The Raman spectra recorded in a mixed solvent of DMC and MA with 1 M LiClO₄ showed an interesting

change when 50-150 Å of Li films were deposited on the smooth Ag surface. Several Raman bands, including 451, 489, and 868 cm^{-1} , are unrelated to the bands from the solvent and supporting electrolytes, and they may be due to the passive films formed at the Li surface. The Raman spectra recorded for smooth Ag in DMC/1 M LiClO_4 solution also showed several bands (348, 449, 620, 891 and 1101 cm^{-1}), which are unrelated to the solution species and may be due to the passive film formed on the Li surface (the most likely species is Li methyl carbonate). A smooth Ag electrode in the DEC solution (with 1 M LiClO_4) did not show any significant Raman bands after depositing 50-2000 Å Li films, contrary to the observations with DMC solution. The results indicate that the Li surface was much more reactive with DEC than with DMC. The reaction product from Li and DEC may dissolve in the solution. However, the Raman spectra recorded at a smooth Ag surface after the deposition of 50 Å Li film in a mixed solvent of DEC and MF showed several bands from the solvent and supporting electrolytes, as well as a couple of bands (1085 and 1213 cm^{-1}) which may be due to the passive films or decomposition products. The results indicate that the reaction of the Li surface with the DEC was suppressed by adding MF to the DEC solution.

Polymeric Electrolytes for Ambient-Temperature Batteries

G.C. Farrington (University of Pennsylvania)

The objective of this program is to investigate the chemical and electrochemical characteristics of polymeric electrolytes for use in high-specific-energy batteries. The investigations this year focused on exploring the electrochemical characteristics and the thermal and electrochemical stability of new, highly conductive polyether polymer electrolytes formed by radiation cross-linking mixtures of acrylate oligomers containing organic plasticizers and dissolved salts. The plasticizers include PC and poly(ethylene glycol dimethylether) (Poly 500); the salts include LiClO_4 , LiCF_3SO_3 , and LiAsF_6 .

The new Li-ion polymer electrolytes containing PC have room-temperature conductivities on the order of 1.5×10^{-3} S/cm. Even at 0°C the conductivities are quite high, typically greater than 5×10^{-4} S/cm. The substitution of Poly 500 for PC reduces the room temperature conductivity to the range of 10^{-4} S/cm, but imparts better mechanical, thermal, and transport properties to the electrolytes without sacrificing good cyclability.

A detailed study of the thermal stability of two electrolyte compositions, one using PC as the plasticizer and the other using Poly 500, along with different dissolved salts, was carried out. The electrolytes containing PC are much less stable thermally than the electrolytes containing Poly 500. The weight loss at 150°C for electrolytes with Poly 500 is less than 1%, whereas the weight loss of electrolytes with PC is between 22 to 35%. Differential Scanning Calorimetry (DSC) studies showed that electrolytes with PC as the plasticizer are completely amorphous from about -85 to 100°C. Electrolytes containing Poly 500 are completely amorphous at room temperature and above but partially crystalline below 12°C.

The electrolytes containing PC and Poly 500 appeared to be stable chemically in contact with Li metal up to 179°C, an important property for battery applications. However, more extensive studies of both the chemical and electrochemical stability of the electrolytes toward Li metal are needed.

Multi-temperature conductivity measurements using symmetric cells of the type, Li/SPE/Li, showed no hysteresis during heating and cooling cycles regardless of which salts and plasticizers were used. In addition, there was no evidence of a change in conductivity upon repeated thermal cycling. The electrolytes displayed good electrochemical and mechanical characteristics over at least 20-30 Li plating/stripping cycles in cyclic voltammetry experiments.

Solid Polymer Electrolytes for Rechargeable Batteries

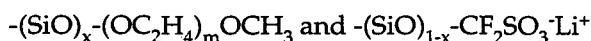
D. Macdonald and S. Narang (SRI International)

The objective of this research is to develop advanced ion-conducting polymers that can be used as SPEs in high-energy-density, rechargeable solid-state batteries. Batteries of this type (e.g., Li/SPE/ TiS_2 , Li/SPE/ V_6O_{13}) have the potential for virtually maintenance-free, reliable operation over hundreds of cycles if certain physicochemical problems can be overcome. Some of the most important technical issues with these batteries are: *i*) low mobility of Li^+ in the SPE, *ii*) difficulty in maintaining intimate contact between the SPE and the Li negative and positive electrodes, *iii*) occasional growth of a Li dendrite that penetrates the SPE on recharging, *iv*) low positive electrode utilization, and *v*) long-term thermal stability at the temperatures at which SPE batteries may operate (e.g., 80-100°C). This project addresses the first point, that is, to develop viable SPEs with higher Li-ion conductivity than that currently available with materials such as poly(ethylene oxide), poly(propylene oxide), and

polyphosphazene. The approach is to synthesize and evaluate new polymer systems having the necessary structural properties to ensure high and stable cation (Li^+) conductivities. Polymers, in which oxygen in the polymer chain is substituted by either nitrogen or sulfur and the addition of other elements, were investigated.

Several sulfur-containing polymers, $[(\text{C}_2\text{H}_4\text{S})(\text{C}_2\text{H}_4\text{O})_x]_n$ ($x = 4, 5, 7, 9, 11, \text{ and } 13$), with sulfur content from 7-20% were synthesized and characterized. Polymer salt complexes were prepared with lithium trifluoromethane sulfonate in tetrahydrofuran. Films of these complexes have been prepared by evaporating the solvent slowly and drying the film thoroughly. As the sulfur content in the polymer decreases from 20 to 10%, the Li^+ -ion conductivity increases from 4×10^{-6} to $7 \times 10^{-6} \text{ S cm}^{-1}$ at room temperature. A further decrease in the sulfur content in the polymer results in a drastic reduction of the ionic conductivity. This observation suggests that the polymer electrolyte having 10% sulfur may have the ideal structure for the transport of ions in the polymer matrix.

Single-ion conducting polymer electrolytes (*i.e.*, polysiloxanes containing perfluorosulfonate pendant groups) with high conductivity at ambient temperature (*e.g.*, $1 \times 10^{-3} \text{ S cm}^{-1}$ for Na^+ -ion conductor) were synthesized. These polymers contain the following pendant groups:



Efforts were concentrated on optimizing the mechanical properties and ionic conductivity of these polymers. Different approaches to the crosslinking of the polymer electrolyte were attempted. A very effective and simple method involved heating the single-ion conductor to 80°C for 2 h. Under these conditions, the viscous liquid transformed into a solid film without any loss in ionic conductivity.

The Li^+ -ion conductivity of the polysiloxanes was measured and found to have one of the highest known conductivities ($1.8 \times 10^{-4} \text{ S cm}^{-1}$ at room temperature after exposure to MeCN). This high conductivity is believed to indicate the separation of ion-pairs in the polymer aggregate having $-\text{COCF}_2\text{SO}_3^-$ groups in the siloxane polymers compared with that of $-\text{CH}_2\text{CF}_2\text{SO}_3^-$ groups in the case of ethyleneimine- or phosphazene-based polymers.

F. CROSS-CUTTING RESEARCH

Cross-cutting research is carried out to address fundamental problems in electrocatalysis, current-

density distribution and gas evolution, solution of which will lead to improved electrode structures and performance in batteries and fuel cells.

Analysis and Simulation of Electrochemical Systems

J.S. Newman (Lawrence Berkeley Laboratory)

The objectives of this project include the investigation of efficient and economical methods for electrochemical energy conversion and storage, development of mathematical models to predict the behavior of electrochemical systems and to identify important process parameters, and experimental verification of the completeness and accuracy of the models. Recent activities are centered on the following areas: *i)* determination of transport properties in sodium polysulfide melts, *ii)* investigations of the formation of salt films on electrochemically active surfaces, *iii)* fundamental studies of the electroprecipitation method for producing Ni electrodes for high-energy batteries, *iv)* impedance analyses of porous electrodes and the dissolution of Cu and Zn, *v)* a mathematical investigation of the transport through and growth of passive oxide films, *vi)* development of boundary-integral techniques for the numerical solution of current and potential distribution problems, *vii)* mathematical modeling of transport processes and experimental determination of transport properties in SPEs, and *viii)* studies of self-generated magnetic fields in high-power batteries.

A model has been developed to predict the response to alternating current of a redox reaction with soluble reactants and products in flow-through porous electrodes. The model accounts for double-layer capacity, and has been compared to experimental behavior. The comparison allows the determination of kinetic and transport properties required for practical system design.

The current and potential distribution on a cylinder embedded in an infinite insulating rod has been solved. The numerical techniques developed here will be applied to practical problems of corrosion protection.

A model for simulating cyclic voltammetry has been modified to account for adsorption of chemical species on the electrode, the chemical or electrochemical reaction of the adsorbed species, and convection transfer. Some questions that need to be addressed in a fundamental investigation of salt films in electrochemical systems are: *i)* How does the film grow?, *ii)* Are the kinetics of film dissolution and precipitation important?, *iii)* Where do film deposition and dissolu-

tion occur, and how do they determine film thickness and porosity? The development of rigorous mathematical models coupled with experimental data is necessary to answer these questions, and thus be able to describe the behavior of electrochemical systems with porous films.

Transport processes play a major role in electrochemical systems. The development of detailed models and the accurate measurement of transport properties are crucial to the improved design of electrochemical cells. Experimental determination of diffusion and conductivity data in sodium polysulfide melts, for example, is vital to enhance the performance of the Na/S cell. Additionally, the theoretical development of transport within polymer electrolytes has lagged. The objectives are to establish a general transport model of the conduction process in these polymers. The model will describe transport phenomena in the polymers under steady-state conditions, subject to a small sinusoidal perturbation, and under transient conditions.

Improvements to the model of a SPE fuel cell were made to include the effects of electrode kinetics and mass transfer to the membrane-electrode interface. Experimental efforts were begun to measure the transport properties of the SPEs as a function of their water content.

The current distribution in a one-dimensional geometry, chosen to approximate that of a bipolar, high-power battery, has been determined. This simple model, based on Maxwell's electrodynamic equations, has provided an estimate of the inductance of the battery as well as the profiles of current in the electrodes.

PUBLICATIONS

1. A.C. West, J.H. Sukamto, and J. Newman, "A Criterion to Verify Current Distribution Calculations," *J. Electrochem. Soc.*, **137**, 2745 (1990).
2. M. Sudoh and J. Newman, "Mathematical Modeling of the Sodium/Iron Chloride Battery," *J. Electrochem. Soc.*, **137**, 876 (1990).
3. J. Newman, "Mass Transport and Potential Distribution in the Geometries of Localized Corrosion," *Perspectives on Corrosion*, AIChE Symposium Series, No. 278, Vol. 86, Geoffrey Prentice and William H. Smyrl, eds. (1990) p. 1.
4. A.C. West and J. Newman, "Determining Current Distributions Governed by Laplace's Equation," LBL-28075 (1990).
5. P.M. Shain, "Cyclic Voltammetry at a Rotating Disk, Electroreduction of Nitrate in Acidic Nickel Solutions, and Frequency-Response Analysis of

Porous Electrodes," *Ph.D. Thesis*, LBL-29118 (1990).

6. A.J. Grabowski, "Current and Potential Distributions on a Cylinder Electrode," *M.S. Thesis*, LBL-29312 (1990).

Surface Layers on Battery Materials

R.H. Muller (Lawrence Berkeley Laboratory)

The purpose of this work is to advance the understanding of properties of surface layers on battery electrode materials that are important for the functioning of rechargeable galvanic cells with high specific energy and power capabilities, energy efficiency, charge retention, and cycle life. Means are sought to achieve superior, predictable properties of surface layers and to form them consistently to provide enhanced battery operation. Present studies are concerned with oxide formation on different metals and the cathodic deposition of Zn from alkaline media.

Anodic surface films that form on Zn in 1 M KOH were studied using Raman spectroscopy. Evidence was obtained for the formation of a Zn(OH)₂ film during the active portion of the anodic potential sweep. In this region the rate of Zn(OH)₂ formation is balanced by its rate of dissolution, and therefore most of the charge ends up as products in the electrolyte and not in the film. Near the active/passive transition potential, the diffusion of hydroxide ions to the metal/film interface becomes rate-limiting, and a film containing kinetically less-favored ZnO is formed. The conductivity of this layer is low, therefore causing a marked decrease in the observed current once the layer is formed. The slow rate of dissolution of ZnO is balanced by its rate of formation.

The structural changes that occur during the cycling of thin nickel oxide electrodes between Ni(II) hydroxide and Ni(III) hydroxide were investigated to identify the reasons for capacity loss and the memory effect in galvanic cells. Evidence for the nucleation of semiconducting oxy-hydroxide in the insulating hydroxide layer was obtained by scanning tunneling microscopy (STM) in Figure 13, and these results are in agreement with the earlier interpretation of transient and spectroscopic ellipsometer measurements. A mechanistic model for the propagation of the phase boundaries during film transformation is being developed.

Intensity-modulated photocurrent measurements were combined with laser Raman spectroscopy and cyclic voltammetry to determine the composition of thin surface oxide layers on Cu which were formed in alkaline media. Photocurrent measurements showed

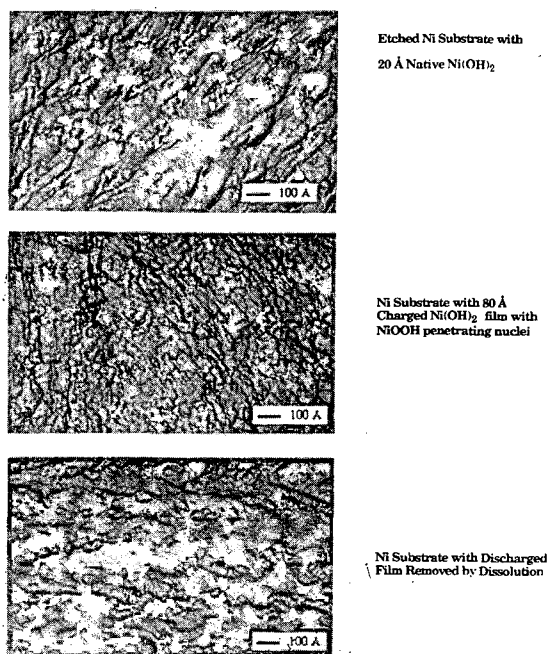


Figure 13. STM images of NiOOH nucleation.
(XBB 917-5126)

that the high-intensity (≤ 250 W/cm²) laser Raman probe beam facilitated reduction of the oxidized surface. Laser-facilitated reduction was used to identify the presence of CuO and Cu(OH)₂ films. Raman spectra confirmed that a thin Cu₂O film formed as oxidation of the Cu surface was initiated. Increasing the potential produced a Cu(OH)₂ layer on top of the Cu₂O film. Further oxidation at higher potentials converted the Cu₂O film to a CuO underlayer that coexisted with the Cu(OH)₂ overlayer.

An illuminated Cu₂O-covered electrode immersed in alkaline media exhibits a nonlinear dependence of photocurrent on the intensity of 488-nm laser illumination. Results from intensity-modulation experiments show that the differential efficiency for converting photons to photocurrent in the p-type Cu₂O film is inversely proportional to the square root of illumination intensity. A charge-transfer model that includes intensity-dependent optical absorption in the Cu₂O layer is found to be consistent with the observed photocurrent response. Analysis of the experimental results using the charge-transfer model shows that the saturation intensity for Cu₂O is ~ 100 mW/cm². Photochemical charge transfer is found to be efficient in the potential region where the nonlinear photocurrent response is observed, with nearly all photo-injected minority carriers being consumed by the interfacial charge-transfer reaction rather than by recombination.

PUBLICATIONS

1. S.T. Mayer and R.H. Muller, "In Situ Laser Raman Spectroscopy of Zinc Film Formation in Alkaline Media." LBL-28116 (1990).
2. D.T. Schwartz and R.H. Muller, "Photoelectrochemical Evidence for Saturated Optical Absorption in Electrolytic Cuprous Oxide," LBL-29661 (1990).
3. D.T. Schwartz and R.H. Muller, "Copper Oxidation Under Intense Illumination - Effects of a Raman Probe Beam," LBL-28218 (1990).
4. D.T. Schwartz and R.H. Muller, "Oxidation Films on Copper in Alkaline Media: Intensity-Modulated Photoelectrochemical and Raman Spectroscopy Studies," LBL-29563 rev. (1990).

Application of Photothermal Deflection Spectroscopy to Electrochemical Interfaces

E.J. Cairns and F.R. McLarnon (Lawrence Berkeley Laboratory)

Photothermal Deflection Spectroscopy (PDS) is being used to study electrochemical interfaces. PDS is a sensitive *in situ* technique which measures the absorption spectrum of the electrode surface and simultaneously detects the concentration gradients formed in the electrolyte. PDS appears to be well-suited for the study of CH₃OH electrooxidation, which is a very slow reaction at the practical operating potentials of fuel-cell anodes. The process by which oxide layers form on Pt was investigated so that the rate-limiting step can be better understood. The initial focus has been the measurement of electrolyte concentration gradients that accompany the formation and removal of oxide films on Pt. The measurements suggest that two phenomena play important roles in Pt oxide film formation: *i*) the movement of H₂O to and from the electrode and *ii*) a non-electrochemical reaction. Water transport is rarely considered in mechanistic studies, however, PDS is sufficiently sensitive to detect small gradients in H₂O concentration near the electrode surface. The ability to detect a non-electrochemical reaction is a powerful feature of PDS. The electrochemist's standard tool, the potentiostat, can detect only electrochemical reactions. Mathematical models of several reaction pathways were used to predict the concentration gradients, and the corresponding electrolyte refractive-index gradients. These predictions were then compared to experimental data. Among the reaction pathways evaluated,

one pathway is strongly preferred: a two-reaction pathway whereby $\text{Pt}(\text{OH})_2$ is formed by an electrochemical step and dehydrates by a chemical step to form PtO . This reaction pathway has an important implication for direct CH_3OH electrooxidation; the dehydration reaction removes O_2 from the electrode surface, which is just the opposite of what is needed for CH_3OH oxidation. Slowing the rate of hydroxide dehydration could improve the overall electrochemical reaction rate for CH_3OH oxidation.

The best CH_3OH electrooxidation rate enhancement has been achieved with Pt-Ru alloy electrodes, and many different mechanisms have been hypothesized to account for its improved activity. The goals of this research are: *i*) a systematic performance assessment of Pt-Ru alloys in several acidic electrolytes, including study of the reported difference between the alloy bulk composition and its surface composition using Auger electron spectroscopy (AES), and *ii*) *in situ* PDS detection of the absorption of infrared radiation by surface species (sub-monolayer coverages). Recently, the precision of the optical alignment procedure of the PDS system was improved, which is needed to make PDS a quantitative technique. Concurrently, an analytical mathematical model describing PDS responses has been developed. The present efforts are directed at advancing PDS into the infrared region of the spectrum, and a thin-layer electrochemical cell has been built for that purpose.

PUBLICATIONS

1. K.A. Striebel, F.R. McLarnon and E.J. Cairns, "Oxygen Reduction on Pt in Aqueous K_2CO_3 and KOH ," *J. Electrochem. Soc.*, **137**, 3351 (1990).
2. K.A. Striebel, F.R. McLarnon and E.J. Cairns, "Fuel Cell Studies in Aqueous K_2CO_3 and KOH ," *J. Electrochem. Soc.*, **137**, 3360 (1990).

Electrode Kinetics and Electrocatalysis of Methanol Electrooxidation

P.N. Ross (Lawrence Berkeley Laboratory)

The objective of this project is to develop an atomic level understanding of the processes taking place in complex electrochemical reactions at electrode surfaces. Physically meaningful mechanistic models are essential for the interpretation of electrode behavior and are useful in directing the research on new classes of materials for electrochemical energy conversion and storage devices.

The best-known catalysts for the direct oxidation of methanol are Pt surfaces modified by underpotential deposition (UPD) of certain admetals, especially Sn. The state of the admetal, valence, number and type of ligand, and coordination to the Pt surface, are all unknown even for the most widely studied systems like Sn. Some studies have speculated that the "active" state of the admetal on Pt is an alloy state produced by electrodeposition of the admetal ions in the electrolyte, others have suggested the active state is an adsorbed (complexed) ion. This question was addressed initially by preparing single-crystal surfaces having adatoms in both a known chemical state and a known atomic position by using ordered Pt_3M alloy surfaces prepared by ultrahigh vacuum (UHV) methods. In the bulk-alloy Pt_3M structure, M atoms are substituted for Pt at the corners of the unit cell. In vacuum, the surfaces of the alloy would ideally have M atoms substituted in an ordered manner for Pt atoms in the surface. It is postulated that the intermetallic bonding in these substitutional positions will stabilize the admetal atoms in these positions in the surface when emersed in electrolyte, and that they will remain in these positions by equilibrium with admetal ions in solution. Studies of methanol electrooxidation kinetics on these ordered surfaces of known composition and structure will enable us to determine the "active" state of the adatom in Pt bimetallic catalysts.

Catalyst surfaces of variable structure and composition were generated by using single-crystal surfaces and UHV preparation techniques, with structure and composition determination being made directly by low energy electron diffraction (LEED) and AES. The activities of the various surfaces for methanol oxidation were measured and correlated to the structure and composition. The stability of the UHV-generated surfaces are confirmed by *ex situ* LEED and AES analyses of the emersed electrodes.

The surface composition and structure of $\langle 111 \rangle$, $\langle 100 \rangle$, and $\langle 110 \rangle$ oriented crystals of the ordered-alloy Pt_3Sn (L_{12} or Cu_3Au -type) were determined using the combination of LEED and low energy ion scattering spectroscopy (LEISS). The clean annealed surfaces displayed LEED patterns and Sn/Pt LEISS intensity ratios which were consistent with the surface structures expected for bulk termination. In the case of the $\langle 100 \rangle$ and $\langle 110 \rangle$ crystals, preferential termination in the mixed (50% Sn) layer was indicated, suggesting this termination is the consequence of a thermodynamic preference for Sn to be at the surface.

To understand the role of Sn as a promoter in the electrochemical oxidation of methanol, the geometric

and electronic effect of Sn atoms in different chemical states on/in the Pt surface was studied by using single-crystal faces of the ordered-alloy Pt₃Sn and single-crystal faces of pure Pt modified by electrodeposited/adsorbed Sn, *i.e.*, the so-called adatom state. None of the alloy surfaces were found to be more effective catalysts than any of the pure Pt surfaces under the conditions of measurement employed here. Furthermore, extensive alloying of Pt with Sn significantly reduced the activity. As reported previously by others, it was also observed that Sn spontaneously adsorbs on Pt surfaces from dilute H₂SO₄ containing Sn(II) in concentrations above ~5 μM. At a given concentration, the coverage by Sn decreased as the atomic density of the Pt surface increased, but methanol oxidation was not enhanced on any of these Pt electrodes that were modified by irreversibly adsorbed Sn. However a diffusion-limited enhancement on Pt(111) and on Pt(100) due to Sn(II) in the electrolyte at 1 μM concentration was observed. At this concentration, Sn did not appear to be adsorbed to any observable extent, and the catalysis appeared to occur *via* the direct interaction of a dissolved Sn species with the surface. A mechanism of catalysis that is a hybrid homogeneous-heterogeneous sequence based on known homogeneous Pt-Sn catalysts is proposed.

PUBLICATIONS

1. U. Bardi, B.C. Beard, and P.N. Ross, "CO Chemisorption on [111] and [100] Oriented Single Crystals of the Alloy CoPt₃," *J. Catalysis*, **124**, 22 (1990).
2. B.C. Beard and P.N. Ross, "The Structure and Activity of Pt-Co Alloys as Oxygen Reduction Electrocatalysts," *J. Electrochem. Soc.*, **137**, 3368 (1990).
3. A. Haner, P.N. Ross, and U. Bardi, "Anomalous Surface Phase Formation on Pt₃Sn <110>," in *Proceedings of the Third International Conference on Structure of Surfaces*, Milwaukee, WI, June 15-20, 1990.
4. P.N. Ross, "Novel Air Electrode for Metal-Air Battery with New Carbon Material and Method for Making Same," *U.S. Patent No. 4,927,718* (May 22, 1990).
5. A. Haner and P.N. Ross, "Electrochemical Oxidation of Methanol on Tin-Modified Platinum Single Crystal Surfaces," LBL-28399 (1990).
6. P.N. Ross, "Characterization of Alloy Electrocatalysts for Direct Oxidation of Methanol," LBL-29435 (1990).
7. A. Haner, P.N. Ross and U. Bardi, "The Surface Structure and Composition of the <111> and <100> Oriented Single Crystals of the Ordered Alloy Pt₃Sn," LBL-28074 (1990).
8. A. Haner, P.N. Ross and U. Bardi, "The Surface Structure and Composition of the Low Index Faces of the Ordered Alloy Pt₃Sn," LBL-29788 (1990).

Engineering Analysis of Gas Evolution

C.W. Tobias (Lawrence Berkeley Laboratory)

The objectives of this project are to elucidate the role of free and forced convection as it affects overpotential behavior and ohmic resistance in electrolytic gas evolution processes, and to clarify the effect of concurrent gas evolution in rechargeable batteries and metal deposition processes. Gas coverage and detachment, as well as behavior in suspension, are usually observed by normal- and high-speed cinematography. In this project, the high-speed interfacial re-equilibration process ("recoil") that is encountered during coalescence of electrolytically-generated bubbles was investigated. The coalescence phenomena between similar (H₂-H₂) or different (H₂-O₂) gas bubbles are observed on precisely aligned microelectrodes facing each other. Spherical bubbles may be evolved at suitably low rates, until they touch and the actual coalescence event which occurs is observed.

Since recoil of typical 200-μm electrolytic bubbles is known to occur in less than 200 μs, and may take place within 10 μs, a high-speed, spatially resolving photodetector was utilized to image the controlled, laser-illuminated coalescence event. By passing a sheet of laser light along the coalescence plane between two bubbles, a bubble-generated shadow is created and focused on the photodetector (Figure 14). The motion of the interface during recoil is then observed by recording the position of the shadow edge at specific time intervals. The photodetector was designed using a fast-response linear photodiode array (50-ns rise time) with high-speed video amplifier and high-speed comparator signal-processing, all coupled to a dedicated data-acquisition unit capable of self-triggering and storing 256 data bits over 16 channels simultaneously at 10 MHz. Thus, 16 elements of the photodiode array may each be sampled at intervals as short as 100 ns.

Results have been obtained for bubbles of 500-1000 μm in diameter. The interface, observed along the coalescence plane, is initially seen to move outward quite rapidly (300-450 cm/s velocities), then

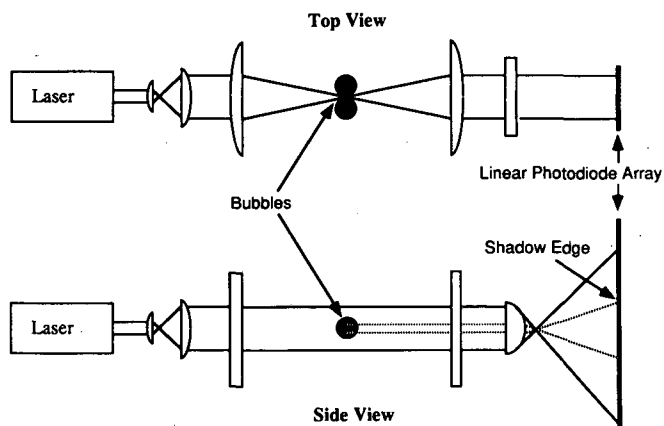


Figure 14. Schematic of experimental design for recoil experiment. Bubbles are formed electrochemically using opposing glass-encased Pt microelectrodes. (XBL 917-1428)

move steadily with the square-root of time (Figure 15). Although the interface is at rest prior to the rupture event which starts the recoil process, the acquired data did not capture any interfacial acceleration; this apparently occurs either in a region below current experimental resolution or entirely within the experimentally inaccessible thin-film region between the bubbles. To provide theoretical justification for the observed square-root time dependence of the motion, a simple model was developed based on the assumption that all of the surface energy is converted to ki-

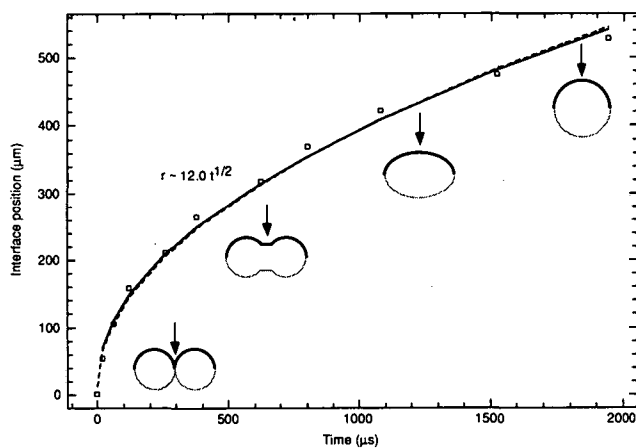


Figure 15. Interfacial recoil transient for two 925- μm diameter hydrogen bubbles. Experiments indicate that the total recoil time is on the order $0.01 r^2$. (XBL 917-1429)

netic energy, an approach previously used by others in thin-film studies. This first-order approximation predicts the observed square-root time dependence.

Smaller, more-realistic bubble sizes (*e.g.*, down to 200- μ diameter) will be studied. Results are also expected for the coalescence of asymmetric bubbles and gas bubbles of different composition (*e.g.*, $\text{H}_2\text{-O}_2$). By taking measurements over various cross-sections of the coalescence event, a complete mapping of the process may be obtained.

IV. AIR SYSTEMS RESEARCH

The objectives of this project element are to identify, characterize, and improve materials for air electrodes; and to identify, evaluate, and initiate development of metal/air battery systems and fuel-cell technology for transportation applications.

A. METAL/AIR CELL RESEARCH

Projects on metal/air cell research address O_2 electrocatalysis; bifunctional air electrodes, which are needed for electrically rechargeable metal/air (Zn/air, Fe/air) cells; and novel alkaline Zn electrode structures, which could be used in either electrically recharged or mechanically recharged cell configurations.

Electrocatalysts for Oxygen Electrodes

E. Yeager (Case Western Reserve University)

The overall objective of this research is to develop more-effective electrocatalysts for O_2 reduction and generation which have high activity and long-term stability. Various electrocatalysts, including the transition-metal macrocycles and oxide catalysts, were evaluated to identify stable catalysts with much higher activity for both monofunctional and bifunctional air electrodes.

Transition-Metal Macrocycles. The structural features of adsorbed transition-metal macrocycles on electrode surfaces are of critical importance to the understanding of how these species function as O_2 electroreduction catalysts. Considerable information has been obtained at CWRU regarding the orientation of the iron and cobalt tetrasulfonated phthalocyanines (TsPc) adsorbed at mono- or sub-monolayer coverages on various substrates using surface enhanced Raman, resonance Raman, uv-vis reflectance, and FT infrared reflectance absorption spectroscopies. Even then, there are questions that still remain unanswered. During the past year, research has been focused on the structural features of the adsorbed monomer and sheet-polymer phthalocyanines on highly ordered pyrolytic graphite (HOPG) using STM, and on lacy carbon using transmission electron microscopy (TEM) at atomic-level resolution.

A high-resolution microscope (JOEL 4000) was used to examine monomer and polymer CuPc and FePc adsorbed on a lacy carbon substrate. Great care

must be taken in adsorbing the macrocycles on the carbon substrates. The preliminary studies have indicated that the structure of the adsorbed layer is more complex than anticipated. Individual molecules are seen and clusters are evident under some circumstances.

The structure of the individual molecules of FeTsPc was examined *ex situ* in air with STM (Digital Instruments, Nanoscope II) adsorbed in multilayers (~100 layers) on HOPG. An STM image showing a crystalline structure was obtained which is similar to the images obtained for chloro-CuPc film (~20-nm thick) by TEM. Based on the x,y offset controlled by STM, the molecules were found to lie on a (001) face and consist of four lobes. Each unit was ~2.0 nm across, indicating the structure of the individual molecules of FeTsPc. Images of monolayer and sub-monolayer adsorption of CoTsPc on HOPG were also obtained by STM in air. The STM images showed that the macrocycle was selectively adsorbed on the HOPG surface. The molecules tend to stack together with the planes of the ligands parallel to each other and adsorb perpendicularly on the surface. Some of the individual molecules were observed lying flat on both the bare HOPG surface and also on top of the stacked layer. Earlier Raman studies at CWRU provided evidence for the perpendicular stacked configuration for TsPc complexes; this structure would not show up well for isolated macrocycles dispersed on the surface. *In situ* STM studies on macrocycles are in progress.

Another phthalocyanine, which was found to be an effective catalyst for the 4-electron direct reduction of O_2 to OH^- in alkaline solution, is iron tetrapyrroline-porphyrazine (FeTPyPz). This phthalocyanine has no net charge and is soluble in acid solution. The cyclic voltammetry of the dissolved and adsorbed species of FeTPyPz on ordinary pyrolytic graphite (OPG) was examined in de-aerated 0.1 M H_2SO_4 . The interaction of the adsorbed macrocycle with the substrate is expected to cause a substantial difference in the redox behavior of the dissolved and adsorbed species. FeTPyPz, similar to FeTsPc, does not show solution phase voltammetry in aqueous electrolyte. This is probably caused by aggregate formation in the solution-phase and extreme broadening of the peaks as a result of resonance splitting.

Studies on the adsorbed layers of dimeric macrocycle designed to test the "dry cave" concept

were initiated during the past year. The important feature of this work is that the cavity formed by the mixture of the oppositely charged water or ethanol soluble macrocycle may be hydrophobic enough to favor the adsorption of O_2 and enhance the kinetics for O_2 reduction. Positively charged tetra kis(4-trimethyl ammonium phenyl) porphyrin (TTAPP) and negatively charged tetra kis(sulfonated) porphyrin (TSPP) with Co ions were synthesized and characterized by uv-visible and diffuse reflectance FTIR spectroscopy. Mixtures of the aqueous solutions of the two oppositely charged porphyrins gave a precipitate that was also characterized by the same spectroscopic techniques. These studies indicated an interaction between the macrocycles through sulfonic and ammonium phenyl groups. Cyclic voltammetry and O_2 reduction electrocatalytic activity for these monomers and their dimer, adsorbed on HOPG surface, are under investigation.

Transition Metal Oxide Catalysts. Ruthenium-containing pyrochlores have shown good activity for O_2 reduction and generation in concentrated alkaline solutions. To gain further understanding of the nature of Ru in various compounds as an electrocatalyst for O_2 reduction and generation, a series of Fe-Ru perovskite oxides with the general formula $SrFe_xRu_{1-x}O_{3-y}$ was synthesized following the nitrate decomposition method at $750^\circ C$. X-ray diffraction showed the presence of single-phase perovskites. In terms of physical properties, this series exhibits variations in electronic conductivity and magnetic behavior. For example, $SrRuO_3$ is at least one order of magnitude higher in conductivity than $SrFeO_3$, although both are metallic conductors. Furthermore, both are paramagnetic at room temperature and above.

The O_2 -reduction kinetics, as well as the rate of peroxide decomposition, increased as x decreased, i.e., as the ratio of Ru/Fe increased in the series. Although these perovskites are not found to be as good as ruthenium pyrochlore catalysts for O_2 reduction and generation, they can be used also as supports for other promising electrocatalysts including macrocycles.

From the cyclic voltammetry of Ru metal it was found that an oxide film formed on Ru when the potential was scanned in the positive direction from the hydrogen adsorption and generation region. The oxide film was not completely reduced when the sweep was reversed. The rotating ring-disk experiments showed that the reduction of O_2 proceeds by a 4-electron pathway on Ru metal. The mechanism and kinetics depend on the oxidation state of the Ru surface.

Various reaction mechanisms for the formation of the anodic film and O_2 reduction on Ru metal are being analyzed.

Bifunctional Oxygen Electrodes. The stoichiometric lead ruthenate pyrochlore, $Pb_2Ru_2O_{7-y}$, continues to be of interest as a bifunctional O_2 electrocatalyst. Further work on this compound was carried out to characterize the catalyst samples by TEM and microdiffraction.

One sample was previously prepared using the alkaline solution method described by Horowitz and co-workers (1). It has been used in a number of gas-fed electrodes with carbon substrates, as well as electrodes without carbon. These electrodes have been found to be particularly stable while retaining good catalytic activity. The TEM showed that the catalyst particles are mostly in the 90-135 nm diameter range with many of them showing flat faces and sharp corners. Some are hexagonal-like and others are more square-like. There were also some much smaller particles of the order of ~10-nm diameter. Microdiffraction was done on several particles and the patterns were indexed. They are consistent with the cubic pyrochlore structure, and they have the correct lattice parameters.

REFERENCE

1. H.S. Horowitz, J.M. Longo and J.T. Lewandowski, *Mater. Res. Bull.*, **16**, 489 (1981).

PUBLICATIONS

1. D. Chu, D. Gervasio, M. Razaq and E. B. Yeager, "Infrared Reflectance Absorption Spectroscopy (IRRAS). Study of the Thermal Stability of Perfluorinated Sulphonic Acid Ionomers on Pt," *J. Appl. Electrochem.*, **20**, 157 (1990).
2. I.T. Bae, D. Scherson and E.B. Yeager, "Infrared Spectroscopic Determination of pH Changes in Diffusionally Decoupled Thin-Layer Electrochemical Cells," *Anal. Chem.*, **62**, 45 (1990).
3. J. Prakash, D. Tryk and E.B. Yeager, "Electrocatalysts for Oxygen Electrodes in Fuel Cells and Water Electrolyzers for Space Applications," *J. Power Sources*, **29**, 413 (1990).
4. D. Ohms, S. Gupta, D. A. Tryk, E. Yeager and K. Wiesener, "ESCA and Electrochemical Studies of Chelate-Modified Carbon Materials for Cathode Oxygen Reduction," *Zeitschrift Physikalische Chemie*, **271**, 451 (1990).

Electrical and Electrochemical Behavior of Particulate Electrodes

J.W. Evans (Lawrence Berkeley Laboratory)

The purpose of this research is to investigate the electrochemical behavior of Zn/air cells that utilize particulate Zn electrodes. The Zn (or Zn-coated) particles form a stationary bed, and electrolyte flow through this electrode occurs by natural convection. The cathode is a monofunctional air electrode that is available commercially.

The success of laboratory-scale cells (up to 400 cm² in cross-sectional area) employing particulate Zn electrodes mandates an investigation of how such cells may be scaled up to a battery for use in EVs. The laboratory cells contain commercially available air electrodes (designed for use in Al/air cells) and do not require an electrolyte pump, the necessary circulation of electrolyte being achieved by natural convection driven by concentration gradients. Scale-up will be facilitated by further experimental investigation, coupled with mathematical modeling of the cell. The following are to be studied:

- i) Solutal natural convection in a cell with a packed-bed or porous electrode.
- ii) Regeneration of the particles (probably in a fluidized bed) by electrodeposition of Zn from spent electrolyte.
- iii) Long-term performance of air electrodes and other cell components such as diaphragms on exposure to alkaline zincate solutions.
- iv) The effect of various vehicle driving cycles on cell performance.
- v) Pragmatic questions, such as how the spent particles and electrolyte are best removed from the cell and replaced with fresh ones.
- vi) The capability of the electrolyte to accommodate the Zn discharge products which has proven to be unusually high in laboratory cells; because this is a major parameter in determining the specific power and energy of a Zn/air cell, this phenomenon requires further investigation.

Testing of laboratory cells (80-cm² air electrode area) with particulate Zn electrodes is continuing. The emphasis of the experimental study has been on testing under discharge following the SFUDS regi-

men. A paper design study for a battery for an EV was completed. Extrapolating laboratory performance under SFUDS discharge, assuming the power and energy per unit area of electrode would remain constant on scale-up, a minimum peak power of 97 W/kg and specific energy of 110 Wh/kg were predicted for this battery.

Laboratory experiments have shown that the mechanical evacuation/refilling of the cell with electrolyte and particles can be carried out. A cell with a fluidized-bed electrode has been constructed and used to deposit Zn from alkaline zincate electrolytes onto particles. Energy consumptions have been as low as 2.3 kWh/kg Zn, thereby demonstrating that particles can be regenerated without excessive energy costs. The particles regenerated by fluidized-bed electrolysis have been shown to perform well on discharge. The commercially available air electrodes (from Electromedia Corporation) that have been used throughout most of this work are undergoing long-term exposure tests to alkaline zincate solution.

A novel feature of the Zn/air cell under investigation is its use of solutal natural convection, rather than forced circulation brought about by an external pump. The flow is an important phenomenon since it removes discharge products from the porous electrode, supplies fresh electrolyte and provides cooling. Use of natural convection eliminates the added capital cost, energy loss, complexity and maintenance that accompany the use of an external pump. Furthermore, shunt currents that may be present with flowing electrolyte in a battery manifold are avoided. A laser-Doppler velocimetry system has been modified to measure electrolyte velocities in the laboratory cell. The results of measurements will be compared with predictions of a mathematical model for flow, mass transport and reaction that is presently under development. The mathematical model, having been tested and refined, will be an effective means of optimizing the cell performance, for example, with respect to particle size.

PUBLICATIONS

1. J. W. Evans and G. Savaskan, "A Zinc-Air Cell With a Packed Bed Anode, Intended for Electric Vehicle Applications," LBL-30079 (1990).
2. J.W. Evans and G. Savaskan, "A Zinc-Air Cell Employing a Packed Bed Anode," LBL-28290 (1990).

Zinc/Air Battery Development for Electric Vehicles

R.A. Putt (MATSI, INC.)

A rechargeable Zn/air battery is being developed for EV propulsion. The key feature of the battery design in this program is a reticulated, flow-through Zn electrode which was conceived at LBL. The life-limiting phenomena of the Zn electrode (*i.e.*, densification, dendrite growth) have been obviated by this invention which employs a macroporous, metal-foam substrate for the Zn electrodeposition. The electrolyte is circulated through the porous structure to supply and remove soluble Zn ions for the electrode reaction.

The objectives of the current program are to verify the long cycle life of this electrode and to transfer the technology to an industrial development program. Substantial progress was made in 1990 in the four key areas of cycle testing, separator development, substrate preplating, and system design.

The cycle testing program has progressed to the point of trouble-free, routine, and hands-off cycling of the Zn electrode in "zinc/zinc" half-cells and laboratory-scale Zn/air cells. These cells are cycled in a 6-h charge, 6-h discharge mode for many months with extremely steady performance. Cycling is performed at DODs between 50 and 100%, with the cells showing tolerance to both partial and complete discharge. The current efficiencies of the Zn electrodes are essentially 100%. The Zn/air cells employ bifunctional O₂ electrodes which, while not the subject of this program, have demonstrated satisfactory electrochemical performance with no failures to date. The success of the cycle testing program is partially the result of a key discovery this year that a higher KOH concentration, 45 wt%, is beneficial for obtaining high surface area and electroactive Zn deposits rather than dense, inactive deposits which result in eventual electrode failure.

The separator development effort during 1990 led to the qualification of a Celgard separator. After extensive evaluation of various combinations of separator materials, a separator comprising 2 or 3 layers of Celgard 3401 microporous polypropylene was shown to be chemically stable and effective in preventing penetration by Zn dendrites. The tests showed that one layer alone is penetrated by Zn dendrites in less than 30 cycles, ostensibly at faults and imperfections in the material, while the use of 2 or 3 layers essentially eliminates the probability of a continuous fault path through the separator. Even 3 layers can be forcibly penetrated by Zn dendrites, but only at high current densities during charge (>20 mA/cm²) and high

capacity densities (>150 mAh/cm² on each side of the Zn electrode), both well above the design values of 5 mA/cm² and 36 mAh/cm².

The Cu-foam substrate for the Zn electrode must be protected from irreversible oxidation in the cell when the electrode is taken to full discharge. During 1990, a number of protective coatings (*e.g.*, Cd, Pb, Sn, Hg) were evaluated as alternatives to the dense Zn preplate developed in the prior year. None of the alternative coatings showed an improvement over Zn, and Hg in particular proved very deleterious to Zn electrode performance. Its presence resulted in dense, hard, and nodular Zn electrode deposits which were electrochemically inactive and which penetrated the separator. Dense Zn has therefore remained as the preplate of choice.

The system design study conducted to estimate the performance of a Zn/air battery for the IDSEP van mission indicated a specific energy of 90 Wh/kg, a system density of 1 kg/l, and a specific power of 90 W/kg.

B. FUEL CELL RESEARCH

Fuel cell research includes projects in several areas of electrochemistry: theoretical studies, fuel-cell testing, fuel processing, and fuel-cell component characterization.

Fuel Cells For Renewable Applications

S. Gottesfeld (Los Alamos National Laboratory)

The primary focus of the Fuel Cell Program at LANL is on the development of polymer-electrolyte-membrane (PEM) fuel cells for transportation applications. The specific goals of the program are: *i*) to reduce the cost of the Pt catalyst and ionomeric membrane, *ii*) to increase the efficiency and power density of the PEM fuel cell, *iii*) to optimize the system for operation on reformed organic fuels and air, and *iv*) to achieve stable, efficient, long-term operation.

Electrode Characterization and Optimization in PEM Fuel Cells. A novel minicell was developed to study the kinetics of the O₂ reduction reaction at the Pt/recast-Nafion interface. The rate of O₂ reduction at a Pt/recast ionomer interface of well-defined surface area was measured to determine the catalyst utilization in a PEM fuel cell. The technique uses a Pt microelectrode covered with recast Nafion, which is a polished disk of 100 μm-diameter Pt wire embedded in the center of a glass rod. The counter electrode is a Pt ribbon held tightly to the side of the rod by a heat-shrunk tubing. The reference electrode consists of a

humidified Nafion tube, which connects the minicell to a separate (aqueous H_2SO_4) compartment containing a dynamic hydrogen electrode (DHE). The minicell is completed by applying a solution of the ionomer (e.g., 5% Nafion solution) to the polished surface of the rod, forming a thin recast film of the ionomer on the Pt microdisk and ionically connecting the Pt to the edges of the counter electrode and the Nafion tubing. The O_2 reduction process at the Pt/recast ionomer interface is studied with the complete minicell "hanging in the air," i.e., in contact with only the humidified reactant gas under conditions identical to those of a PEM fuel cell.

The current and potential were measured at various temperatures and with an atmosphere of O_2 and saturated water vapor at a total pressure of 1 atm. It was found that both the interfacial kinetic and mass transport rates increase with an increase in temperatures between 7 and 40°C. However, the kinetics becomes more sluggish as the temperature of equilibration increases above 40°C. The O_2 reduction performance of a minicell equilibrated with saturated water vapor at 80°C is poor. A Tafel plot of the mass-transport corrected current density at 30°C shows a slope of ~100 mV/decade in the range 0.9 to 0.8 V, and a higher slope of ~140 mV/decade in the range 0.7 to 0.4 V. To understand the poor performance at higher equilibration temperatures, the minicell was immersed in liquid water and the current-potential curve recorded for the fully immersed electrode at 80°C. The catalytic activity at 0.9 V for the immersed electrode was quite high, whereas, as expected, the mass-transport rate was limited. Following this immersion step, the electrode was emersed from the liquid but maintained in the saturated vapor above the liquid water at 80°C. At times longer than 30 min after electrode emersion the O_2 reduction kinetics became more sluggish. This is apparently caused by loss of water from the film.

These results are very important for fully understanding the role of water and optimizing the humidification of PEM fuel cells. They clearly showed that *i*) the interfacial kinetics—not only the protonic conductivity—is adversely affected by the loss of water from the recast Nafion electrolyte, and *ii*) that the recast Nafion loses water when transferred from liquid water to saturated water vapor equilibrated with the liquid. The former conclusion seems to be at odds with some previous ideas on the possible importance of Nafion as a "dry cage" for enhancing O_2 reduction. It could be clearly seen that the O_2 reduction kinetics are faster at higher water contents (although an excessive interfacial water content can apparently be reached).

Based on a current density of 0.2 mA/cm² measured for O_2 reduction at 0.9 V ($P_{\text{O}_2} = 1$ atm) for the Pt/recast Nafion model interface, the calculated catalyst utilization achieved with assemblies containing Prototech electrodes (0.45 mg Pt/cm² loading) is close to 10%. This calculation is based on an overall Pt surface area according to TEM examination of 600 cm² Pt/cm² geometric, and the measured fuel cell activity at 0.9 V of 60 mA/cm² at 5 atm O_2 . An assumption made in such evaluations of catalyst utilization is that the interfacial activity per unit surface area of the supported-Pt catalyst is the same as that of bulk Pt. However, it is not clear whether the particle of the electrocatalyst should be considered chemically and structurally identical to bulk Pt. To answer this question a series of measurements of x-ray absorption (EXAFS and XANES) on samples of carbon-supported Pt catalysts was initiated. Preliminary results suggest that the catalyst particles are actually quite different from bulk Pt in both their chemistry and their degree of crystalline order. The information obtained to date has demonstrated the capability of these x-ray absorption techniques to clarify structural and compositional details of complex samples of highly dispersed-supported-Pt catalysts.

Water Transport in Polymer Electrolyte Membranes. This year the first series of nuclear magnetic resonance (NMR) measurements of the proton (¹H) self-diffusion coefficient in Nafion membranes of different well-defined states of hydration was completed. The diffusion coefficient of water in Nafion and related membranes is a necessary input to model the water behavior in fuel cells using these membranes. Changes in the water diffusion coefficient with varying water content is important for Nafion-based PEM fuel cells since they are usually operated under conditions of partial hydration of the polymer. The level of hydration could also vary with position across the membrane when the cell is under load. Calculation of the water profile across the ionomeric membrane in a cell at steady state thus requires knowledge of water diffusion coefficients as a function of water content.

In the pulsed-field-gradient, spin-echo (PGSE) NMR experiments, the self-diffusion coefficient of the species with the detected nucleus is determined from the diffusional dephasing of a gradient-encoded magnetization. Experimentally, a pair of symmetrically spaced field gradient pulses is placed into a normal spin-echo sequence. The additional signal attenuation as a function of the strength of the field gradient pulses yields the self-diffusion coefficient of the species of interest. The measured self-diffusion coefficients are summarized in Table 2 as a function of water content. The ¹H intradiffusion coefficients in

Nafion decrease with decreasing water content. To determine whether two distinct types of water with different diffusion rates are present in the membrane, experiments are conducted with a second field gradient. As shown in Table 3, the measured diffusion coefficients are independent of the value of this second field gradient, indicating that no dispersion in the diffusion rates of ^1H nuclei exist in the sample. Thus, we conclude that no large "pockets" of bulk water (e.g., water-filled bubbles in the membrane) are detectable under the conditions of these experiments.

It is important to note that the measured diffusion coefficient is not necessarily the self diffusion coefficient of water in these membranes. The identification of the ^1H diffusion coefficient with that of water is reasonable at high water contents since $^1\text{H}_2\text{O}$ is in excess over $^1\text{H}^+$. At low water contents, we have found that a diffusion coefficient estimated from conductivity measurements is virtually identical with that measured for ^1H by NMR methods. We conclude that in this extreme H_2O and H^+ diffuse together. The measured diffusion coefficient of ^1H nuclei is thus a good estimate of the water diffusion coefficient in the membrane over the full range of water contents.

We also determined the diffusion coefficient in the presence of a chemical potential (water concentration) gradient by using water activity *vs* water content data to correct the measured self-diffusion coefficients. As shown in Table 4, the resulting "chemical diffusion coefficients" show a much smaller range of variation with water content than do the self-diffusion coefficients. These results show the power of NMR for determining the diffusion coefficients of water (^1H) in PEMs.

Table 2. ^1H Intradiffusion Coefficients, 30°C

Water Content ($\text{H}_2\text{O}/\text{SO}_3\text{H}$)	$D (\times 10^6, \text{cm}^2/\text{sec})$
2	0.6 ± 0.06 (SDE*)
3	1.2 ± 0.08 (SDE)
4	2.1 ± 0.06 (SDE)
6	3.7 ± 0.15
9	4.4 ± 0.07
14	4.9 ± 0.43

* The label SDE indicates that this diffusion coefficient was determined using the SDE-PGSE technique.

Table 3. Effect of Gradient Strength on D Measured by SDE-PGSE Experiment

Gradient Strength (G/cm^2)	$D (\times 10^6, \text{cm}^2/\text{sec})$
0	3.6 ± 0.3
2.38	4.0 ± 0.3
4.76	3.9 ± 0.2
7.14	4.3 ± 0.2
9.52	3.3 ± 0.4

Table 4. Chemical Diffusion Coefficients

Water Content ($\text{H}_2\text{O}/\text{SO}_3\text{H}$)	$D_{\text{chem}} (\times 10^6, \text{cm}^2/\text{sec})$
2	1.8
3	2.0
4	2.1
6	1.5
9	1.1
14	2.8

PEM Fuel Cell Model. A one-dimensional model was developed which describes the complete PEM fuel cell. It is the first model which relies fully on a complete set of experimentally derived transport properties for the ionomeric membrane. The one-dimensional steady-state model for water transport through a complete PEM fuel cell includes transport of water and reactant gases through the porous electrodes, based on calculated diffusivities corrected for porosity. The transport of water and protons through the membrane electrolyte are based on experimentally determined water sorption isotherms (by isopiestic equilibration), water diffusion coefficients (by NMR), electroosmotic drag coefficients (measured in a special cell with Pd(H) electrodes in contact with the membrane), and membrane protonic conductivities. All of these transport properties were measured as functions of membrane water content. We deemed it highly desirable to use a complete set of experimental data in the model that is generated under conditions in which the membrane-electrode assembly is routinely treated and tested in PEM fuel cells. Because of the variation of the water content as a function of po-

sition within the membrane during fuel cell operation, all of these properties had to be experimentally evaluated as functions of membrane water content. An important question in the model concerned the boundary conditions at the membrane-electrode interfaces. The assumptions made were that the equilibrium water activity at these interfaces determines the local water content at the membrane surface. The experimentally determined isotherm for water sorption into the membrane was used to convert from water vapor activity to water content in the membrane at the electrode-membrane interface. The water activity at the cathode-membrane interface was always near unity. For the anode-membrane interface, the number of water molecules carried into the membrane per proton produced was iterated in the computer code until the equilibrium conditions at the other (membrane-cathode) interface were satisfied. This approach provides a measure of the net flux of water through the cell per proton passing through the membrane.

The results generated by the model are shown in Figures 16 and 17. Figure 16 shows the calculated water profiles with a Nafion 117 membrane at four different current densities. It shows that the electroosmotic water drag causes a local depletion of water near the anode which becomes more severe at higher current densities. Figure 17 shows the calculated effect of membrane thickness on cell performance for Nafion 1100 membranes. It demonstrates the significant nonlinear effect achieved by thinning the membrane down to 50 μm . It also demonstrates an impor-

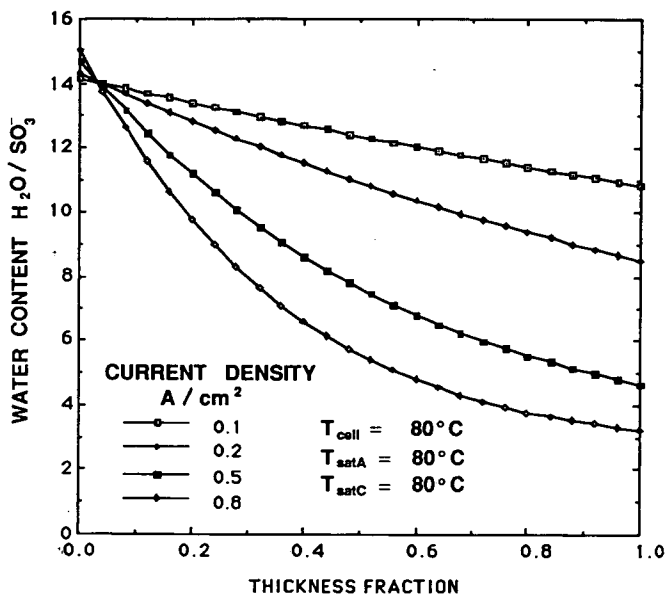


Figure 16. Water profiles for Nafion 117 membrane calculated from mathematical model. (XBL 917-1430)

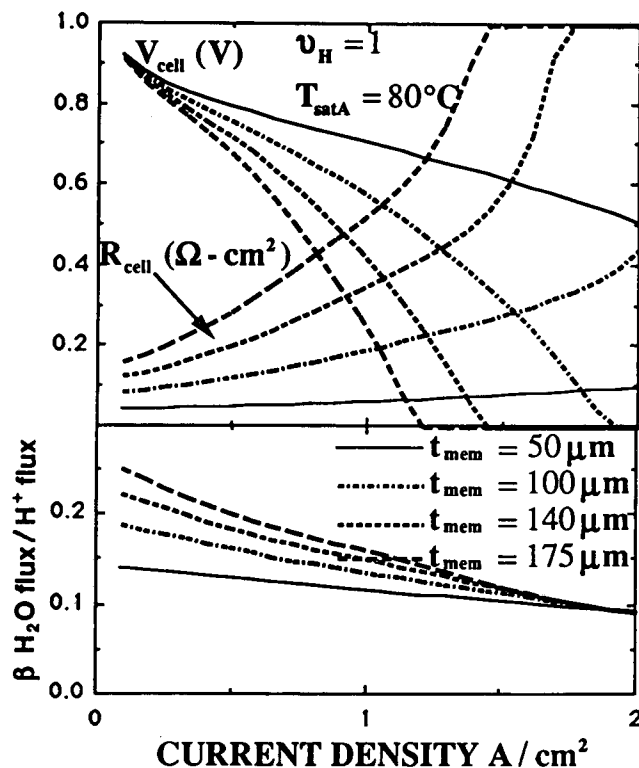


Figure 17. Effect of Nafion 117 membrane thickness on cell performance. (XBL 917-1431)

tant finding from the model that the net flux of water per proton (0.1-0.2 $\text{H}^+/\text{H}_2\text{O}$) is expected to be much smaller than the electroosmotic drag measured through a membrane immersed in liquid water (typically 2.5 $\text{H}^+/\text{H}_2\text{O}$). The model is useful for predicting the performances of PEM fuel cells based on other ionomeric membranes for which the same set of experimentally derived data can be generated.

Endurance Testing and Materials Stability. This year we completed the fabrication of six new fuel cell test stations which replaced existing hardware employed in our single-cell testing facility. The new test stations incorporate all the features required for safe, continuous, computer-controlled testing of single polymer-electrolyte fuel cells or small stacks of such cells under pressure and elevated temperature. Each test station is an integrated unit that controls gas flow, pressure, and humidity cell and gas temperatures. It also reads and/or controls cell voltage and current.

The test station incorporates a HP 6060JA electronic load in series with a 5 V, 12 A power supply. The power supply provides a voltage boost for the electronic load enabling it to reach higher currents. The electronic load, which is controlled by a computer, can be operated in either constant-current or constant-voltage mode. The test station has an auto-

matic gas shut-off feature where two solenoid valves are actuated by an over-temperature switch within the thermocouple controller for the fuel cell. The over-temperature is set to 35°C which allows the change in operation of a cell from 80°C (standard operating temperature) to 50°C (standby mode) without gas shut down. In the event of gas crossover and a fire within the cell, the 35°C differential will be quickly surpassed and the gases will be shut off.

Life tests were performed on pressurized (H₂/air) PEM fuel cells with 5-cm² active area in the new test station at 80°C and with the reactant gases humidified at 105°C. This cell employed 0.45 mg Pt/cm² on each (Prototech) carbon cloth electrode, and a 5-mil thick ionomeric membrane (Membrane C, Chlorine Engineers, Japan). The electrode impregnation and membrane-electrode hot-pressing conditions were those previously optimized at LANL. The cell employed a pressurized "bladder" to maintain uniform mechanical pressure across the electrode-membrane contact area. The bladder pressure was varied in the range 250-400 psi, producing significant effects on cell performance. The cell operated continuously without any interruption during the full period of testing. During most of the test the cell operated on air (5 atm) and hydrogen (3 atm), and at a constant voltage of 0.5 V and current densities of 0.60 to 0.75 A/cm². The cathode performance on O₂ was established at the beginning of the test for comparison. The cell was also operated on O₂ (5 atm) for a few days in the middle of the test period during an interruption of the pressurized air supply in the building.

No sustained degradation was observed in the performance of this cell during the 2100 h of testing, which was terminated by equipment failure. Indeed, a 25% improvement in performance was recorded as the test proceeded. This result indicates that long-term operation of PEM fuel cells with low Pt loading will not be a problem. The test also demonstrated the advantages of the new fuel cell test stations.

During the past year, tests performed by International Fuel Cells (IFC) with low-Pt loading membrane-electrode assemblies (M&EA) prepared at LANL verified the performance obtained at LANL. The M&EA are based on impregnated Prototech electrodes which are hot-pressed onto ionomeric membranes of the "Membrane C" type (manufactured by Chlorine Engineers). The tests at IFC were performed on assemblies with an active area of 2" x 2" (26 cm²), as compared with the 5-cm² electrodes employed in most of the tests at LANL. IFC also fabricated and tested assemblies based on Prototech electrodes with low-Pt loading (0.5-0.6 mg/cm²) and other experimental ionomeric membranes.

The results of the IFC tests can be summarized as follows (quoting in some places directly from the IFC reports):

1. "The test results were positive in two important respects: *i*) they showed that the Los Alamos performance using low loaded electrodes could be repeated in IFC 2" x 2" cells, and *ii*) they showed that the alternate 'Membrane C' gave performance comparable to other experimental membranes, thus qualifying another source (of membranes)."
2. A new bonding condition was used by IFC but "the performance of the M&EA was poor and, upon disassembly of the cell the electrodes delaminated cleanly from the membrane. The same electrodes were then rebonded to a fresh sample of the membrane, but this time using conditions specified by LANL. The electrodes were strongly bonded to the membrane and the M&EA performed well."
3. It was found by IFC that an important prerequisite to obtain the LANL-quoted performance in their tests was to apply a strong mechanical pressure (strong "pinch") across the assembly. The spacing between the ribs could also have a significant effect (35-mil spacing is used in the hardware at LANL and subsequently adopted in the tests at IFC). Their conclusion has been that the strong "pinch" is necessary for obtaining good mechanical support with the relatively soft carbon-cloth electrode material in these assemblies.
4. It was found that an increase in air flow and switching from humidified to dry air were prerequisites for achieving cell currents well in excess of 1 A/cm².

Advanced Chemistry and Materials for Fuel Cells

J. McBreen (Brookhaven National Laboratory)

The purpose of this work is to increase the understanding of electrocatalysis on a molecular level and to apply this knowledge to fuel cells. The goals of this project are to reduce the Pt requirements in PEM fuel cells, and to develop non-Pt catalysts for O₂ reduction and the direct oxidation of methanol. Work in 1990 included *i*) EXAFS studies of UPD Sn on carbon-supported Pt in acid electrolytes, and *ii*) XANES studies of Pt catalysts poisoned by methanol oxidation products.

EXAFS studies of Pt/UPD Sn Electrocatalysts. Early

in the year a new cell was designed and built for obtaining *in situ* EXAFS spectra on dilute catalysts in the fluorescence mode. This cell was successfully used in studies of UPD Sn on carbon-supported fuel cell catalysts (Prototech) in 0.5 M $\text{H}_2\text{SO}_4 + 2 \times 10^{-3}$ M SnCl_4 . The electrode was held at 0.0 V (*vs* a saturated calomel electrode [SCE]) for 8 h to deposit the UPD Sn, and EXAFS measurements were made in the fluorescence mode over a potential range of -0.24 to 0.30 V. The Fourier transforms of the Sn EXAFS, at the two extremes of potential, revealed: *i*) at 0.3 V only one peak was observed at 0.15 nm, attributed to the Sn-O interaction; and *ii*) at -0.24 V the Sn-O interaction was much less and other peaks at 0.25 and 0.35 nm from Sn-Pt interactions were observed. The Fourier transforms change smoothly with varying potentials from those found at the extremes. So far these studies indicate that UPD Sn differs from other UPD metals in that it remains on Pt over a wide potential range and its interaction with oxygen varies in a continuous and reversible fashion with potential. These are most probably the features that make it a good catalyst for direct oxidation of methanol. The labile O_2 may oxidize CO poisons.

XANES Studies of Methanol Oxidation. The XANES study included *in situ* measurements on carbon-supported Pt in pure 0.5 M H_2SO_4 and in 0.5 M $\text{H}_2\text{SO}_4 + 1$ M CH_3OH . Electrodes were made from Teflon-bonded (12% PTFE) Prototech catalyst. The electrodes were operated in the flooded mode and were first characterized in 0.5 M H_2SO_4 using cyclic voltammetry. XANES spectra were recorded at several potentials. The electrodes were transferred to a 0.5 M $\text{H}_2\text{SO}_4 + 1$ M CH_3OH electrolyte, and the spectra were recorded after the electrodes were at open

circuit for 1 h. Methanol was oxidized at 5 mA/cm² for 2 h and another set of XANES spectra were recorded. In pure acid the spectrum in the double-layer region corresponds closely to that for Pt metal. In the hydrogen adsorption region there is a broadening on the high-energy side of the white-line peak. Similar effects have been found in the case of gas-phase hydrogen adsorption on Pt catalysts. On open circuit, in the solutions containing methanol, there is a broadening of the white line similar to that found in pure acid in the hydrogen adsorption region. After methanol oxidation there is an increase in white-line intensity at lower energies. This indicates that the poison causes a depletion in d-band electrons in the Pt. On open circuit, in the presence of methanol, the surface is covered mainly by hydrogen produced by the dissociation of methanol. Hence, the spectrum is similar to that found in pure acid in the hydrogen adsorption region. It is only after methanol oxidation that there is a buildup of the poison. The strong effect of the poison on the electronic structure of the Pt is indicative of the chemical nature of the Pt-poison interaction.

PUBLICATIONS

1. J. McBreen, W. E. O'Grady, G. Tourillon, E. Dartyge and A. Fontaine, "XANES Study of Underpotential Deposited Copper on Carbon Supported Platinum, BNL-45350 (1990).
2. J. McBreen, "XAS Techniques for Investigation of Materials for Energy Conversion and Storage," BNL-44841 (1990); to be published in *Electrochemistry in Transition*, O.J. Murphy, S. Srinivasan and B.E. Conway, eds., Plenum Press, New York.

LAWRENCE BERKELEY LABORATORY
UNIVERSITY OF CALIFORNIA
INFORMATION RESOURCES DEPARTMENT
BERKELEY, CALIFORNIA 94720